A TRANSIENT METHOD OF MEASURING THERMAL

CONTACT CONDUCTANCE BETWEEN METAL-PLASTIC

SURFACES

by

RAMALINGAM THARMALINGAM

A Thesis

Submitted for the Degree of

Master of Science

Awarded the degree of M.Phil.

Department of Chemical Engineering,
The University of Aston in Birmingham,
Birmingham, UK

September 1972

SUMMARY

The thesis describes a method developed to measure thermal contact conductance between metal-plastics surfaces by transient experiments. Published literature contains no comparable transient experimental technique and no conductance values for metal-plastics surfaces. Thermal transients set up by a radiant heat flux in two aluminium alloy rods which sandwich between them a thin sheet of plastic material are used to evaluate the contact conductance.

Crank-Nicolson's finite difference scheme is used to evaluate the time-temperature history in a three body composite system with contact resistance at two interfaces. The details of the experimental equipment designed and constructed for this work is presented. Dimensionless groups obtained from the heat conduction equation, initial and boundary conditions predict the contact conductance from experimental data and the limits to the accuracy of the measurements of contact conductance. Optimisation techniques are used to find the minimum of the sum of squares function formed by the theoretically predicted and experimentally measured temperature values. The thermal conductivity of the plastic material is also evaluated from these measurements.

The thermal contact conductance values obtained by this method at various applied pressures lie in the range of 40 BTU/hr ft^2 $^\circ$F (227.2 W/m^2 $^\circ$K) to 200 BTU/hr ft^2 $^\circ$F (1136 W/m^2 $^\circ$K) and the thermal conductivity of the plastic material was 0.1042 BTU/hr ft $^\circ$F (0.1803 W/m $^\circ$K). This conductivity value agrees with that given in the literature.

The effects of applied pressure and ambient pressure on contact conductance are investigated.

ACKNOWLEDGEMENTS

CONTENTS

LIST OF FIGURES

LIST OF SYMBOLS

α Thermal diffusivity

β Modulus $= \dfrac{\alpha \cdot \Delta\Theta}{(\Delta x)^2}$

c Specific heat

F_o Heat flux at $x = o$

h_c Contact conductance

K Thermal conductivity

K_p Thermal conductivity of the plastic material

l Length

m Thickness of the plastic material

n Subscript

Q Heat loss correction term

ρ Density

T Temperature

T_F Furnace temperature

T_i Initial temperature

Θ Time

$\Delta\Theta$ Time step

X Distance

Other symbols appearing are defined in the text.

S E C T I O N   1

INTRODUCTION

The objective of this work is to develop a transient method to measure thermal contact conductance at metal-plastic interfaces. The thesis presents theoretical and experimental investigations of the transient temperature in a one-dimensional three-body composite system with contact resistance at two interfaces. The method and results are of use in the field of plastics technology, in curing calculations, injection moulding and other applications where heat passes across metal-plastics interfaces. The results will be also of interest in comparing the theories of contact conductance because the surfaces considered for the present work differ so greatly in their physical properties.

A majority of the previous workers on contact conductance measurements carried out theoretical and experimental investigations on metal-metal contacts to give information for the thermal design of space vehicles (re-entry vehicle, heat shield), nuclear reactors, electronic equipment and so on, and have shown that contact resistance may be significant. The models investigated by them mainly consisted of two-body composite systems. For the present work a three-body composite system was chosen due to the difficulties in measuring temperature in plastic materials. All temperature measurements were made in two metal rods which sandwich between them a thin sheet of plastic material.

Previous work has shown that steady state experiments need very accurate temperature measurements at several points on both sides of the interface. The location of thermocouples very close to the interface would cause disturbances in the interface

region ·2

interstitial volume

constriction of
heat flowlines

interstitial
heat transfer

region 1

solid solid
conduction
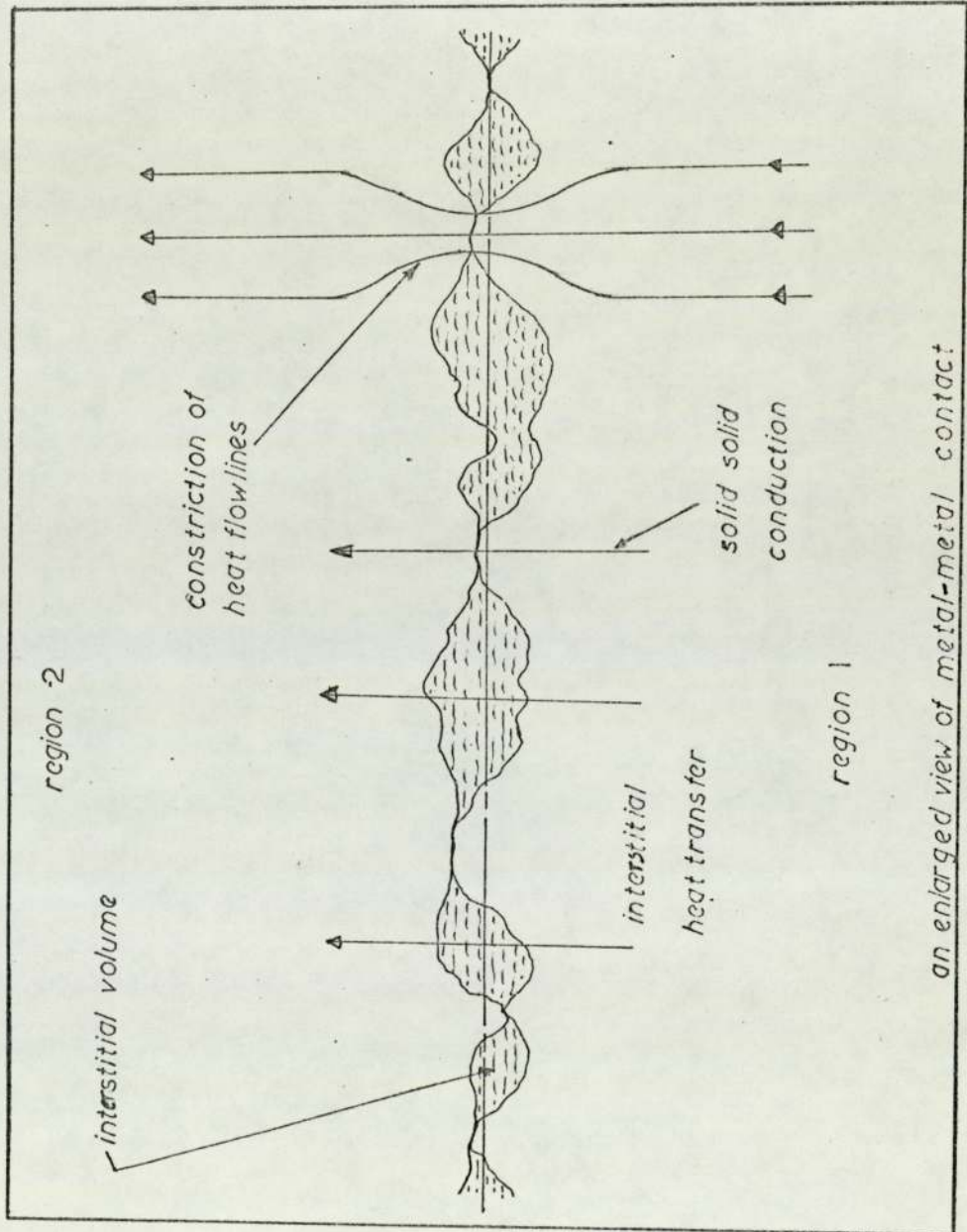
an enlarged view of metal-metal contact

FIG 1.1a

temperature and hence the extrapolation of temperature profiles becomes inevitable in steady state measurements. Also, it requires a very stable sink to maintain the boundary temperature value constant. However, for transient techniques the equipment could be made simpler and more reliable. Temperature measurements have to be accurate but an adequate time-temperature history can be obtained with fewer thermocouples.

Basic concepts of contact heat transfer are discussed in the remainder of this section. Section 2 examines some of the literature in the field of contact conductance, and transient experimental techniques relevant to this work. The mathematical model used and the theoretical studies made are explained in Section 3. The description of the experimental equipment designed and constructed for this work and the experimental procedure employed in the measurements are presented in Section 4. Section 5 gives the results obtained and a discussion of the accuracy of the method developed.

Contact conductance studies are basically concerned with the flow of heat near the interfaces of two solid bodies in contact. Nominally flat surfaces which appear to be smooth are actually rough (on a microscopic level) and make contact at discrete points as shown in Figure 1.1a. (This illustration is representative of metal-metal contact). The bodies touch each other only where the peaks touch peaks or peaks touch valleys. The total area of contact may be less than 1% of the cross-section area and is above 20% only for carefully prepared surfaces [6, 30]. However, in a metal-plastics contact due to the lower hardness of the plastic material, the contact spots will be larger in number

FIG 1.1b

an enlarged view of metal - plastics contact

region 1 (metal)

solid solid
conduction

interstitial
heat transfer

constriction of
heat flow lines

interstitial volume   region 2 (plastics)
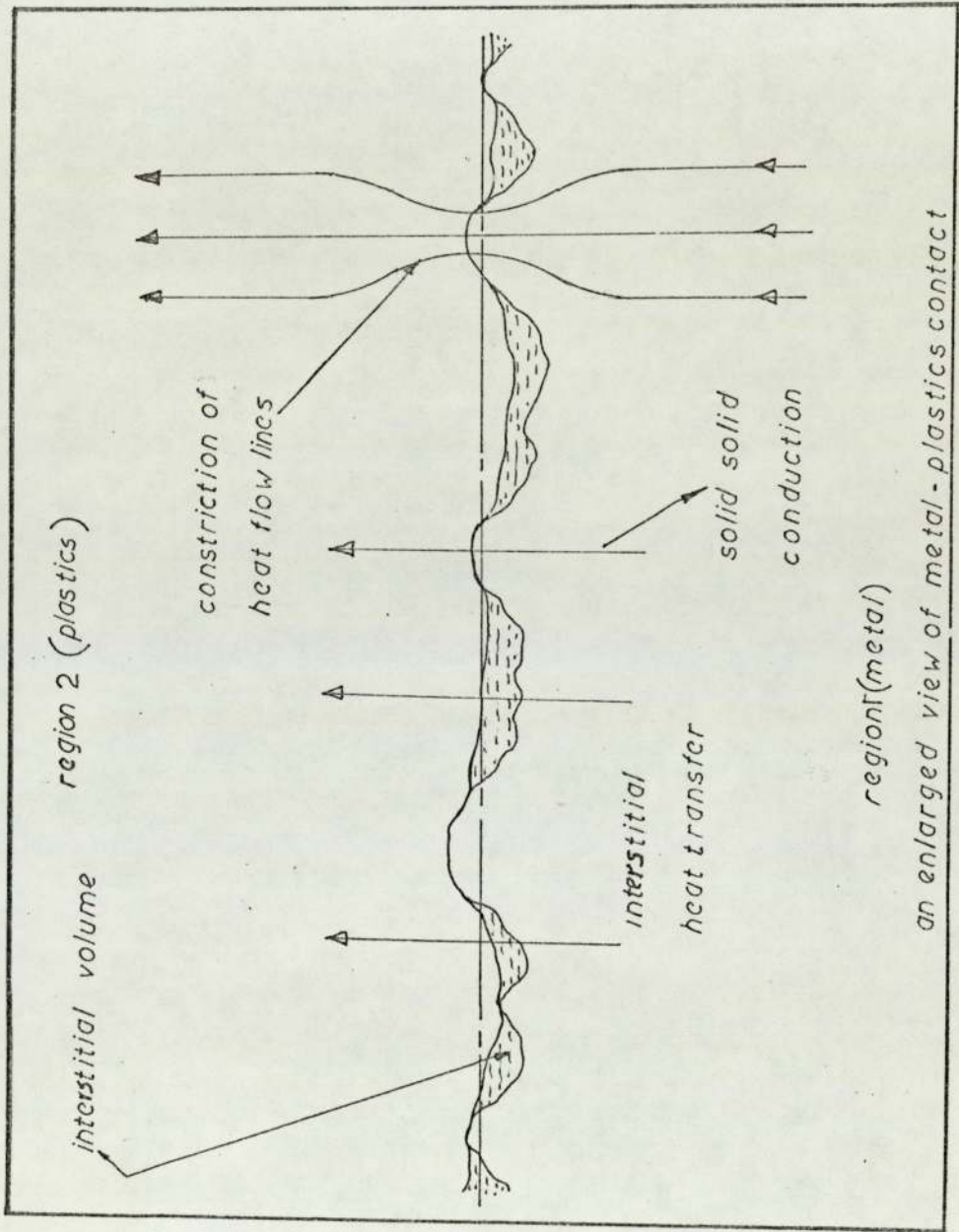
compared to that in a metal-metal contact and hence the contact area will be relatively higher. When the contact pressure is increased the plastic material will deform into the interstitial volume and will increase the contact conductance.

An enlarged view of metal-plastics surfaces in contact can be represented by Figure 1.1b. (p 4)

Definition of Contact Conductance

Thermal contact conductance h_c is defined as

$$h_c = \frac{Q_c}{A_c . \Delta T_c} \quad (W/m^2 \; {}^{\circ}K) \qquad (1.1)$$

where Q_c = Heat flux across the contact

A_c = Cross-sectional area of the surfaces in contact

ΔT_c = Temperature drop at the contact

The definition of the temperature drop at the contact of a composite system under steady state conditions is illustrated in Figure 1.2a. The temperature profile on either side of the contact will be a straight line and ΔT_c is usually obtained by extrapolating the profiles up to the interfaces. Under transient conditions, however, the shape of the profiles will depend on the initial and boundary conditions and time, Θ. Figure 1.2b illustrates the temperature profile under transient conditions if the system is insulated and heated at one end.from an initially uniform temperature for time Θ. This is based on the theoretical studies made in this work. Direct measurement of ΔT_c (by extrapolation of the temperature profiles) will not be required in the transient method.

Temperature Profile under Transient Conditions

FIG 1.2b

Temperature Profile under Steady State Conditions
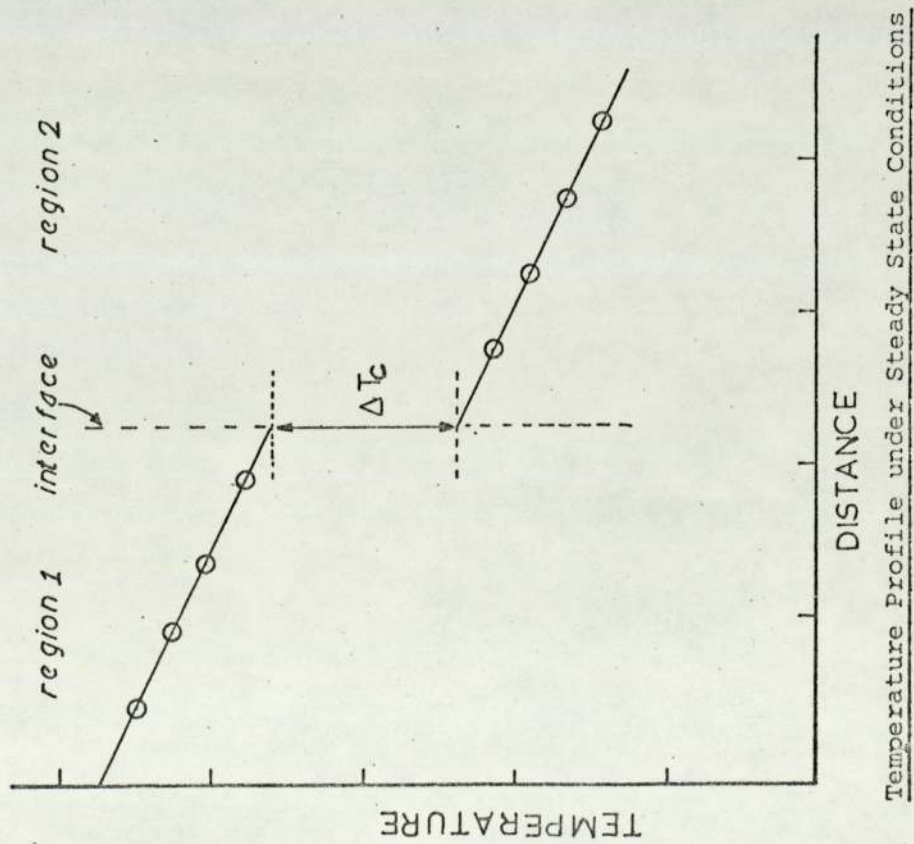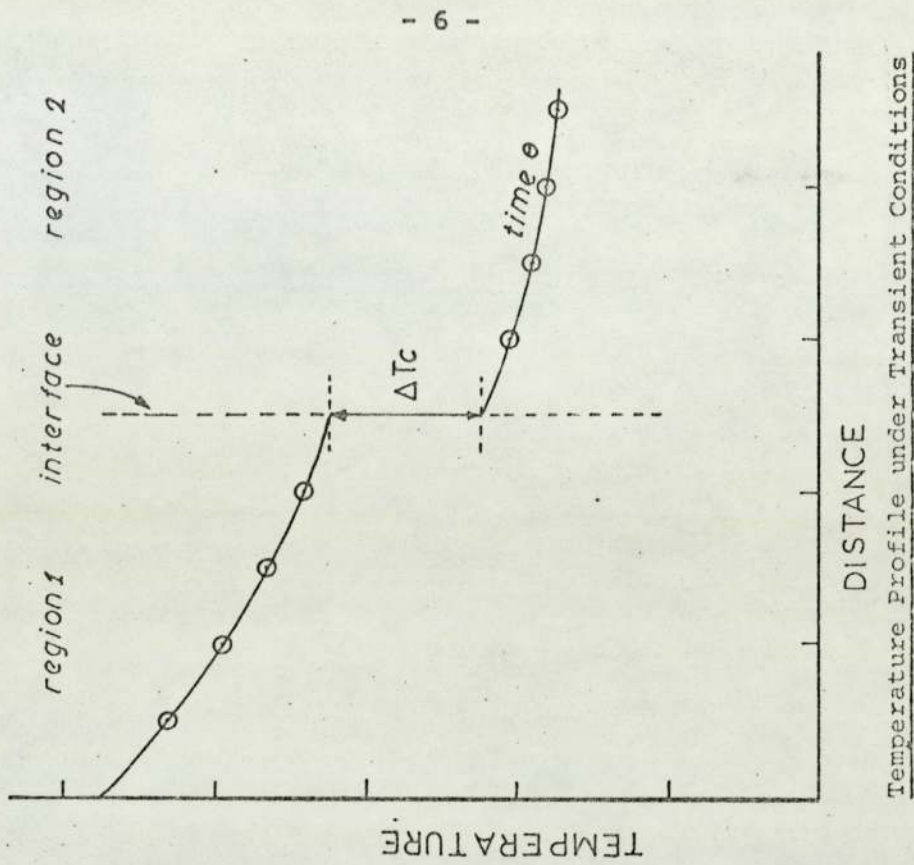
FIG 1.2a

Four mechanisms which may contribute to the heat transfer between surfaces in contact are:

(i) Conduction through the contact points

(ii) Convection through the fluid in the interstitial volume

(iii) Conduction through the fluid in the interstitial volume

(iv) Radiation between the contacting surfaces

The relative importance of these mechanisms depends on a number of factors including the hardness and roughness of the surfaces, the applied pressure and the properties of the fluid between the contacts.

<u>S E C T I O N   2</u>

LITERATURE SURVEY

The aim of this section is to present some of the literature relevent to the present work including publications on contact conductance measurements and transient experimental techniques. The majority of the early work published on contact conductance was presented by authors who were interested in the measurement of thermal conductivity. In the field of contact heat transfer, very little work has been published, and no work published so far includes any measurements of contact conductance at metal-plastic interfaces or of conductance for surfaces of widely different hardness.

2.1 Convective and Radiative Heat Transfer

The theoretical solutions reported by the earlier workers were based on idealised models. Several models are reported for the four somewhat independent modes of heat transfer. Most of the authors $[3, 5, 10, 18]$ assumed that the contact points are widely distributed, such that the radii of the contact spots are small compared to the distance between them and the gap thickness δ_f is small compared to the distance between them. The model is illustrated in Figure 2.1. This model for the convective mode, was based on two parallel flat plates separated by a distance δ_f. Three different orientations of the plates were considered by the authors. However, they concluded that the convective heat transfer across a contact can be safely ignored for any realistic problem. For a metal-plastic contact these assumptions may be equally valid.

Fenech and Rohsenow $[10]$ have estimated the radiative heat

Idealised Contact Model
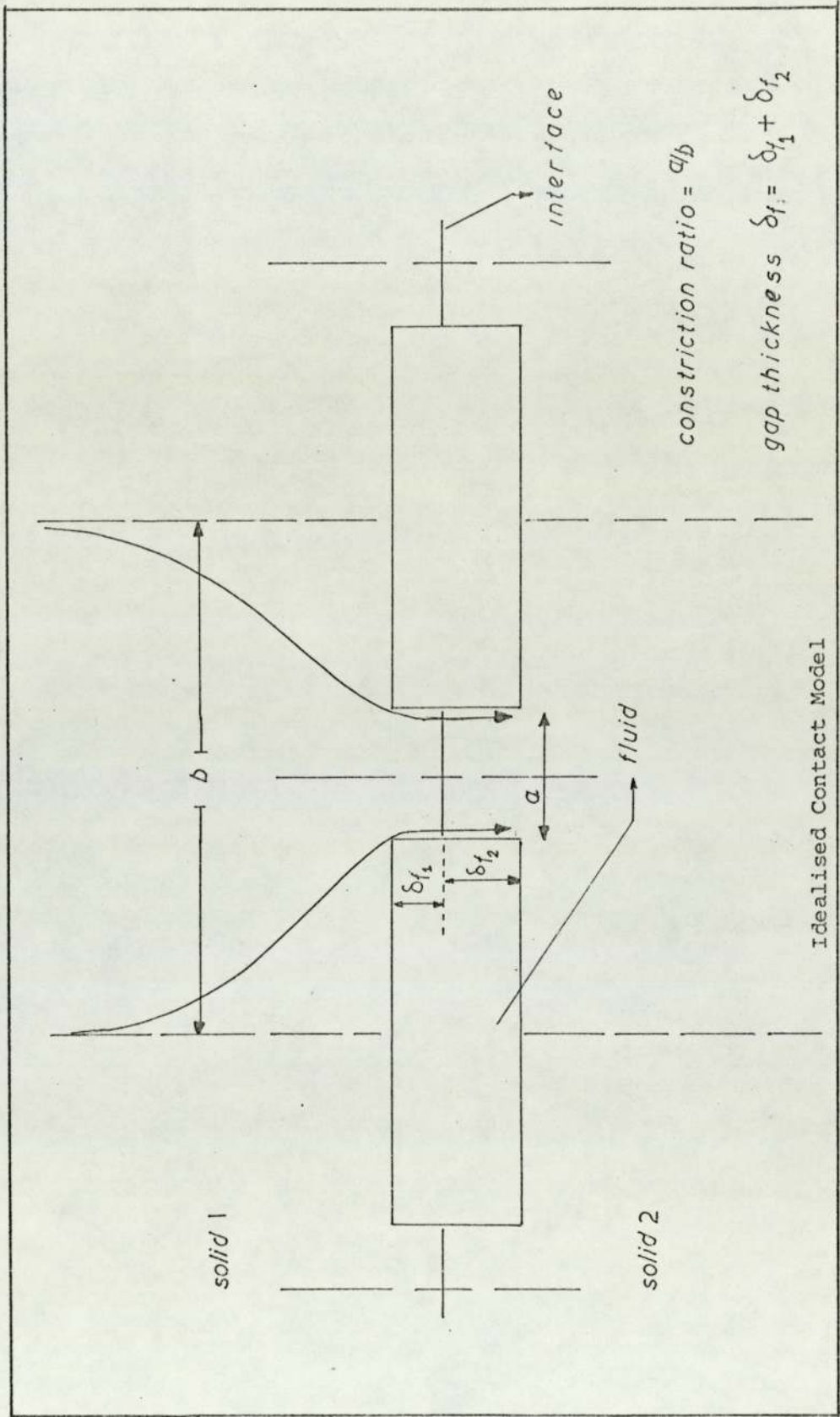
FIG 2.1

transfer contribution to the total to be less than 1% for mean contact temperatures below 1100°F. Clausing and Chao [5] have reported that the radiation amounts to less than 2% of the total in the least favourable conditions of their experimental work. Moore [6], in order to estimate the gap radiation, has assumed the interface temperature drop ΔT_c, to be small compared to the mean temperature and obtained the following expression for the radiative conductance h_r:

$$h_r \simeq 4 \, E_{12} \, \sigma \, Tm^2 \qquad (2.1)$$

in which

$$E_{12} = \frac{1}{\dfrac{1}{E_1} + \dfrac{1}{E_2} - 1} \qquad (2.2)$$

E_1 and E_2 are the emissivities of the surfaces.

$Tm = \dfrac{T_1 + T_2}{2}$ and σ is the Stefan-Boltzmann Constant.

Moore also estimated the radiation to be less than 2% of the total, even at the lowest conductance of 29 BTU/hr ft^2 $^\circ$F he has measured.

2.2 Fluid Conductance

The two modes of heat transfer that contribute mainly to the resistance are the solid-solid conduction and the conduction through the fluid. The fluid conductance h_f is defined as:

$$h_f = \frac{K_f}{\delta_f} \qquad (2.3)$$

where K_f = conductivity of the fluid

δ_f = Effective gap thickness

Early work [30] reports that fluid conductance may even account for over half the total conductance. For metal-plastic contact this case would arise only under extremely high surface roughness of the metal and very low contact pressures. Equation 2.3 suggests that the fluid conductance h_f can be increased by introducing a high conductivity fluid in the interstices.

The evaluation of δ_f in a metal-metal contact itself is a difficult task. In metal-plastics contact, assuming the surface of the plastic material to be perfectly smooth, the variation of the gap thickness δ_f with contact pressure will be very difficult to predict. However, the contribution of the fluid conductance, h_f, to the total can be roughly estimated from conductance values measured at constant contact pressure and different ambient pressures.

2.3.1 Solid Conductance

Solid-solid conduction mode, h_s, contributes a major proportion to the total conductance h_c under normal circumstances. The heat flow lines must converge to pass through the contact spots. Moore [6] has used the term 'constriction resistance' or 'constriction conductance' for the constriction of heat flow lines. A surface will mainly have two types of irregularities: the surface waviness which is macroscopic and surface roughness which is microscopic. Hence two types of constriction of heat flow lines result. Firstly, due to the macroscopic waviness the heat flow lines converge to pass through the macroscopic contact areas and then converge again to pass through

the microscopic contact spots.

Several models are available for the prediction of constriction ratio a/b (Figure 2.1) to estimate solid-solid conduction mode for metal-metal contacts. They differ in the assumptions made by the respective authors.

2.3.2 Deformation Analysis

In order to predict the solid conduction mode, a relationship between the applied pressure and the constriction ratio a/b, (Figure 2.1), is essential. When normally rough surfaces are pressed together, the actual area of contact between them will be a small fraction of the cross-sectional area. Hence, the average pressure on a contact spot will be much higher than the applied pressure. The softer of the two materials will tend to deform elastically or plastically, or both elastically and plastically.

If the deformation is assumed to be plastic and the pressure on a contact is equal to the maximum which can be sustained by the softer material (called the Meyer hardness value M) then using a simple force balance

$$P.A_c = M A_s$$

P = Applied pressure

A_c = Cross-sectional area

A_s = Actual contact area.

Hence:

$$\frac{a}{b} = \sqrt{\frac{A_s}{A_c}} = \sqrt{\frac{P}{M}} \qquad (2.4)$$

If the deformation is assumed to be partially elastic, the
average pressure borne by an a-spot will be a fraction of the
Meyer hardness, M, i.e. the pressure on an a-spot P_a is:

$$P_a = \xi.M \qquad 0 < \xi < 1 \qquad (2.5)$$

hence

$$\frac{a}{b} = \sqrt{\frac{P}{\xi.M}} \qquad (2.6)$$

The above two assumptions were used by earlier workers in building
up their models.

2.3.3 Microscropic Contact Models

Cetinkale and Fishenden [3] used the model shown in
Figure 2.1 to predict values of contact conductance. The
contact element was assumed to be a circular cylinder of
radius b, with a centrally placed solid spot of radius a,
surrounded by a fluid of thickness δ_f. The heat transfer was
assumed to occur through the contact and through the surrounding
fluid by conduction. The steady temperature distribution in
the model was obtained by the relaxation method, controlled by
the dimensionless quantities a/b and $b.K_f/\delta_f.K_m$. They have
obtained solutions for ten different cases to include practially
all real cases (including the special case of a/b = 0, in
which the flow will be linear throughout the cylinder.) The
authors arrived at the following relationship after some
rearrangements:

$$h_s = \frac{\left[\frac{a}{b}\right].K_m}{b.K_f \tan^{-1}\left[\frac{b}{a}\middle/\left[1 - K_f/(h_s.\delta_f)\right] - 1\right]} \qquad (2.7)$$

in which K_m = harmonic mean of K_1 and K_2. Since h_s appears on both sides of the equation, an iterative method was used to evaluate h_s.

In order to evaluate a/b, the authors assumed the deformation of the a-spots to be completely plastic, hence from equation (2.4):

$$\frac{a}{b} = \sqrt{\frac{P}{M}}$$

Also the authors have suggested means by which the gap thickness δ_f and the heat channel radius b can be evaluated from surface roughness measurements and some experimentally measurable constants. They concluded that conductances between specially smoothened and roughened surfaces can be estimated with sufficient accuracy for practical purposes using these equations and the experimental values of δ_f and b.

Laming [18] employed the model given in Figure 2.1. He assumed for normally flat, rough surfaces which are only just in contact, the a-spots, whether few or numerous, must be vanishingly small owing to very small radii of curvature of roughness peaks. If the surfaces are pressed together under an increasing load, the a-spots will increase in size, firstly due to elastic then due to plastic deformation. Supported by the previous work, that the elastic deformations are negligible except for very smooth surfaces, Laming consequently assumed as Cetinkale [3] and obtained:

$$a = \left[\frac{1}{N\pi} \cdot \frac{P}{M}\right]^{\frac{1}{2}} \qquad (2.8)$$

in which N = Number of a-spots per unit nominal area.

Laming then used the conclusion of Holm [34] that con-
ductance of a single a-spot is 2 a K_m. This is based on the
assumption that the dimension of 'a' is small compared with b,
the effective radius of the region supplying each a-spot. Then
to account for ~~in~~ those cases when high loads are applied, where the fluid
and solid conductivities become comparable, he modified the
relation to apply to single finite size a-spot by the use of a
'constriction alleviation factor', f, where:

$$h_{a-spot} = \frac{2 \ a \ K_m}{1 - f} \tag{2.9}$$

where f is a function of a/b such that $f \to 1$ as $a/b \to 1$.

Laming approximated (1 - f) to the first two terms in Rosse's
series such that:

$$f = 1.41 \left[\frac{a}{b} \right] \tag{2.10}$$

He assumed that the surfaces will have a regularly pitched
waviness in one direction (due to mechining) and the number of
contact points is equal to the number of ridge intersections.
Eventually he arrived at the following expression for h_s, the
solid conduction mode, (from equations (2.8) and (2.9)):

$$h_s = \frac{2 \ K_m}{1 - f} \left[\frac{\text{Sin } \alpha}{\pi . \lambda_1 . \lambda_2} \ \frac{P}{M} \right]^{\frac{1}{2}} \tag{2.11}$$

where λ_1 and λ_2 are the surface wave lengths and α the angle at
which the ridges are oriented. Hence, the total conductance
term h_c becomes:

$$h_c = \frac{K_f}{\delta_f} + \frac{2 \ K_m}{1 - f} \left[\frac{\text{Sin } \alpha}{\pi . \lambda_1 . \lambda_2} \ \frac{P}{M} \right]^{\frac{1}{2}} \tag{2.12}$$

The remaining unknowns are a/b to evaluate f and the value of δ_f. He obtained a/b from the relationship:

$$\frac{a}{b} = \left[\frac{P}{M} \cdot \frac{h_c}{h_s}\right]^{\frac{1}{2}} \qquad (2.13)$$

$$f = 1.41\left[\frac{P}{M} \cdot \frac{h_c}{h_s}\right]^{\frac{1}{2}} \qquad (2.14)$$

Hence, by eliminating f from equations (2.11) and (2.14) h_s can be evaluated which appears implicitly.

Fenech and Rohsenow [10] approached the problem in a similar manner as in [18, 3 and 5] using the model given in Figure 2.1. They obtained the expression for the sum of the fluid conductance and solid conductance as:

$$h = \frac{\frac{K_f}{\delta_f}\left[(1-\epsilon^2)(4.26\sqrt{n}\frac{\delta_1}{\epsilon} + 1 + 4.26\sqrt{n}\frac{\delta_2}{\epsilon} + 1) + 1.1\epsilon \; f(\epsilon) \; \frac{1}{K_1} + \frac{1}{K_2}\right] + 4.26 \; \epsilon\sqrt{n}}{(1-\epsilon^2)\left[1 - \frac{K_f}{\delta_f}\frac{\delta_1}{K_1} + \frac{\delta_2}{K_2}\right]\left[\frac{4.26\sqrt{n}\frac{\delta_1}{\epsilon} + 1}{K_1} + \frac{4.26\sqrt{n}\frac{\delta_2}{\epsilon} + 1}{K_2}\right]}$$

$$(2.15)$$

$\epsilon = \sqrt{\frac{A_c}{A}}$ where A_c = real contact area and A = apparent contact area, in which $\epsilon < 0.1$ for all practical surfaces and $f(\epsilon) \simeq 1$. The term in square brackets in the numerator is referred to as the heat flow across the voids and the second fraction as the heat flow through the contacts.

The application of this equation to actual surfaces requires three quantities to be evaluated, δ_f, M and ϵ. For small ϵ, the authors develop the following expression for the average fluid
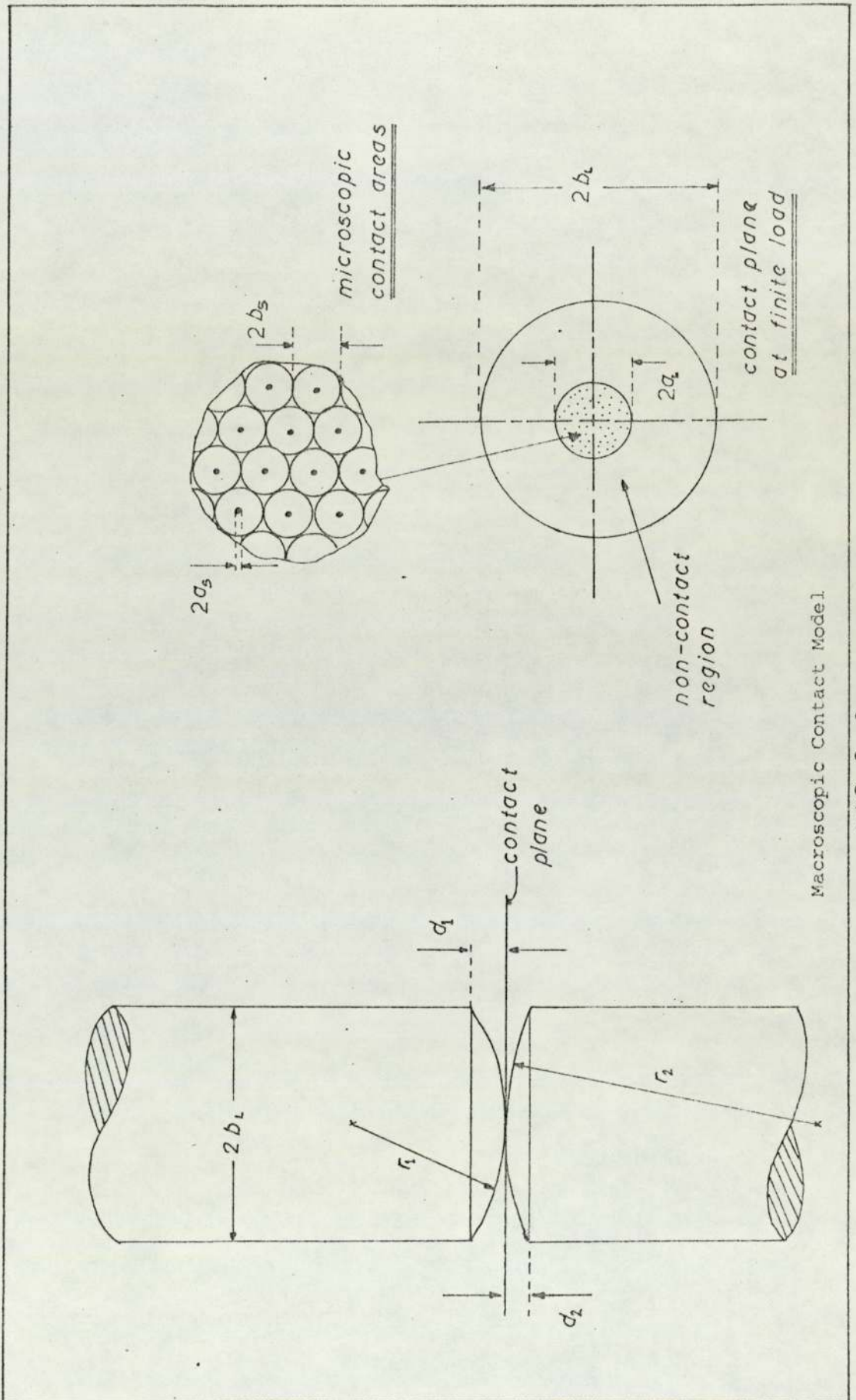
FIG 2.2

Macroscopic Contact Model

thickness:

$$\delta_i = \left[\frac{\xi_i}{1 - \frac{K_f}{K_i}}\right], \quad i = 1, 2 \quad \text{and} \quad K_f \neq K_i \tag{2.16}$$

where ξ = average height of gaps in actual contact. The remaining unknowns n, ϵ, ξ_1 and ξ_2 were obtained from surface profile measurements.

Cooper et al [7] have considered the resistance between two solid thick bodies in vacuum. They have compared the existing analyses of a single idealised contact and applied it to predict conductance of multiple contacts.

2.3.4 Macroscopic Contact Models

Clausing and Chao [5] have demonstrated that for many surfaces used in engineering practice the macroscopic constriction has a commanding influence on the overall resistance. They have presented a model (Figure 2.2) to predict thermal contact con-ductance in a vacuum and have obtained results to show the effect of surface film, surface roughness, creep and interstitial material.

Their model suggests that thermal resistance across a con-tact in the absence of any conducting fluid may be represented by three resistances, R_L, R_S, and R_o in series in which:

R_L = macroscopic constriction resistance (or large scale)

R_S = microscopic constriction resistance (or small scale)

and R_o = film resistance.

Hence, the total resistance $R_t = R_L + R_S + R_o$.

For microscopic resistance based on the model given in Figure 2.1, they derived the same expression as Laming [18]:

$$h_{s_1} = \frac{2_a K_m \cdot n}{g(x)} \tag{2.17}$$

in which h_{s_1} = microscopic conductance

x = (a_s/b_s)

$g(x)$ = Rosses' series

However, they assumed that the asperity deformation is partially elastic and hence the average pressure borne by an a-spot, P_a, is assumed to be a fraction of the Meyer hardness, M.

i.e. $P_a = \xi.M$, $0 < \xi < 1$ as in equation (2.5)

hence

$$h_{s_1} = \frac{2.P.K_m}{\pi.M.\xi.a_s\ g(x)} \tag{2.18}$$

The authors assumed an average value of 0.3 for ξ.

For macroscopic constriction analysis, the authors assumed the contacting portion to be of radius 'a_L' and the heat channel radius to be 'b_L'. The contacting region was assumed to consist of a large number of contact spots, each of radius 'a_s' (Figure 2.2) and obtained the relationship:

$$\frac{h_L.b_L}{K_m} = \frac{2.x_L}{\pi.g(x_L)} \tag{2.19}$$

in which $x_L = a_L/b_L$

h_L = macroscopic conductance.

They assumed the macroscopic resistance to be governed by the elastic deformation of the contacting members. In order to predict the macroscopic contact area and its variation with applied pressure, the flatness deviation of the contacting solids was simulated by spherical caps of radii r_1 and r_2 (Figure 2.2). They eventually obtained the following expression for x_L:

$$x_L = 1.285 \left[\frac{P}{E_m}.\frac{b_L}{d_t}\right]^{\frac{1}{2}} \quad \text{for } x_L < 0.65 \tag{2.20}$$

in which $d_t = d_1 + d_2$ = total flatness deviation.

E_m = harmonic mean of the two modulii of elasticity

E_1 and E_2

The dimensionless group $(P/E_m)(b_L/d_t)$ was designated as ξ and called the conformity modulus.

Hence, from equations (2.17) and (2.18)

$$\frac{h_L \cdot b_L}{K_m} = \emptyset (\zeta) \qquad (2.21)$$

in which

$$\emptyset (\zeta) = \frac{2 \times 1.285\ \zeta^{1/3}}{\pi\ g(1.285\ \zeta^{1/3})} \qquad (2.22)$$

i.e.

$$\frac{h_L \cdot b_L}{K_m} = \frac{2.57\ \zeta^{1/3}}{\pi\ g(1.285\ \zeta^{1/3})} \qquad (2.23)$$

and the ratio of microscopic conductance to macroscopic conductance becomes:

$$\frac{h_{s_1}}{h_L} = \frac{2}{\pi} \cdot \frac{P}{M} \cdot \frac{1}{\emptyset (\zeta)} \cdot \frac{b_L}{a_s\ \xi\ g\ (x)} \qquad (2.24)$$

in which for a given material of known geometry and load, the quantities P, M, ξ and b_L are known. They estimated $a_s.\xi.g\ (x)$ by assuming 'a_s' is independent of the load and the average size of the microscopic contact area is of the same order as the surface roughness.

They have indicated from their calculations that microscopic conductance is of secondary importance for many engineering surfaces.

Popov and Yanin [29] have reported heat transfer studies

between surfaces with waviness. Their model for the macro-deviation is basically the same as that used by Clausing and Chao [5]. They conclude that the wave height and the equivalent out-of-flatness are the governing factors that affect contact resistance. No experimental method is presented but the theoretical values are reported to be in satisfactory agreement with experimental data.

Sanokawa [23] has presented theoretical analysis of a model of contact. The presentation consists of four parts including the effect of the shape of surface roughness and the waviness. He has performed experiments on waviness model and shown that the contact resistance is roughly the sum of the resistances due to roughness and waviness in series. Also, he states that unless extreme care is taken to avoid waviness, there might be many cases in which the resistance due to waviness might exceed that due to roughness.

2.3.5 Comparison of Contact Models

The theories available include only the prediction of contact conductance h_c, for either rough-flat surfaces or smooth-wavy surfaces. Theories on surfaces with a considerable amount of roughness and waviness are yet to be published. The mechanisms suggested by Centinkale and Fishenden, Laming, and Fenech and Robsenow are applicable only for flat-rough surfaces. Out of the work carried out on the microscopic contact model, Laming's method requires less information. Fenech and Robsenow's needs much effort to evaluate some of the parameters but is more accurate. Clausing and Chao's work on macroscopic contact model

will be applicable in preference to the others in cases where
the surfaces will have large scale waviness. Their experimental
results and theory agree for cylindrical specimens with spherical
ends (Figure 2.2), but there is no information regarding the
applicability and accuracy of the solutions for practical cases.

2.4 Transient Methods

Beck [1] has described a procedure for using transient
experimental data to determine simultaneously, several physical
properties appearing in certain partial differential equations.
The properties were estimated by making the temperatures calculated
by finite difference approximation to match the measured temperatures
in a least-squares sense.

Beck [17] also describes a method using non-linear esti-
mation procedure to evaluate contact conductance as a constant or
as a function of time. He suggests that the dimensionless number,
B, where

$$B = \frac{h_c \cdot L}{K} \tag{2.25}$$

in which L = specimen thickness

h_c = contact conductance

K = thermal conductivity.

When less than or equal to 0.5, the location of thermocouples are
not critical.

When B > 0.5, some thermocouples have to be located as near to
the interface as possible, but outside the disturbance layer.

Moore [6] has presented solutions derived for a class of
boundary value problems for transient temperature distribution in

a one-dimensional, two-layer composite rod. These solutions were
an original contribution to the field of contact heat transfer.
The theoretical analysis includes four different cases. In the
section of Literature Survey, he presented a tabulated review of
most of the existing publications on contact conductance studies
and closely related topics, categorised by the type of information
to be found in the various references.

He has reported an effective method of locating thermo-
couples on the surface of the test specimen (explained in Section 4).
The experimental program of Moore consisted of six phases. The
experimental conditions were approximated to the boundary conditions
used for his theoretical solutions. These six phases of the
program differ in the initial and boundary conditions, applied
pressure and ambient pressure. The test samples used included a
large range of thermal properties.

50% of the experimental results obtained are reported to be
within 10% of the predicted values while 20% of them differed from
the predicted values by more than 20%.

Moore recommends a much stabler source block, larger number
of thermocouples and careful surface preparation for future work.

S E C T I O N   3

THEORETICAL

3.1.1 Principle of Transient Method for Thermal Contact Conductance, h_c

        As stated in the Introduction, the work of this thesis

concerned measurements of thermal contact conductance by a transient

method. In the method a constant heat flux causes the temperature

of a composite rod containing a plastic sheet sandwiched between

metal sections to increase, and sets up thermal transients in the

rod. An illustration of the geometry of the composite rod is given

in Figure 3.1.
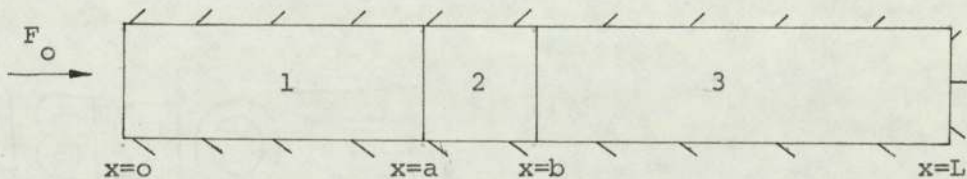
Figure 3.1

All three regions of the rod are assumed to be one-dimensional

with constant thermal properties. The system is well insulated

to reduce the radial heat loss. The temperature distribution in

each of these three regions is assumed to obey the one-dimensional

transient heat conduction equation including the correction term

for the surface heat loss.

3.1.2 Heat Balance over an Element of the Composite Body
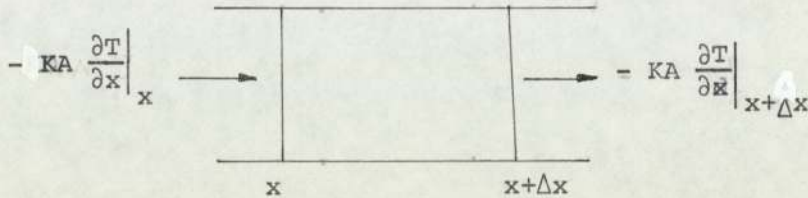
Figure 3.2

For the element (Figure 3.2) x to x + Δx, whose cross-sectional area is A and perimeter P

Rate of accumulation = Rate of input - Rate of output

$$A \cdot \Delta x \cdot \rho \cdot C_p \frac{\partial T}{\partial \Theta} = - K \cdot A \frac{\partial T}{\partial x}\bigg|_x + K \cdot A \cdot \frac{\partial T}{\partial x}\bigg|_{x+\Delta x} - p \cdot \Delta x \, f(T-T_i)$$

(3.1)

in which $f(T-T_i)$ is the rate per unit area of (convection) heat transfer from the surface of the rods.

Taking Limit $\Delta x \to 0$, 3.1 becomes

$$\frac{\partial T}{\partial \Theta} = \frac{K}{\rho \cdot C_p} \frac{\partial^2 T}{\partial x^2} - F(T-T_i)$$

or

$$\frac{\partial T}{\partial \Theta} = \alpha \frac{\partial^2 T}{\partial x^2} - F(T-T_i)$$

(3.2)

Appendix 1 discusses the experimental determination of the value of $F(T-T_i)$ by recording cooling curves of the rods, from which

$$F(T-T_i) = Q.(T-T_i)^2$$

(3.3)

in which Q is a constant.

3.1.3 Mathematical Model

Initially, all three regions of the composite rod are at a uniform unitial temperature T_i. At time $\Theta = 0$, the end $x = 0$ (Figure 3.1) is suddenly exposed to a constant radiant heat source and it receives a constant radiant heat flux F_o. The flow of heat across the interfaces $x = a$ and $x = b$ are assumed to be continuous and no heat flows across at $x = L$.

Hence, the process can be represented by the following mathematical model:

For the first metal rod:

$$\frac{\partial T_1}{\partial \Theta} + Q(T_1 - T_i)^2 = \alpha_1 \frac{\partial^2 T_1}{\partial x^2}, \quad 0 \leqslant x \leqslant a \tag{3.3}$$

For the plastic rod:

$$\frac{\partial T_2}{\partial \Theta} + Q(T_2 - T_i)^2 = \alpha_2 \frac{\partial^2 T_2}{\partial x^2}, \quad a \leqslant x \leqslant b \tag{3.4}$$

For the second metal rod:

$$\frac{\partial T_3}{\partial \Theta} + Q(T_3 - T_i)^2 = \alpha_3 \frac{\partial^2 T_3}{\partial x^2}, \quad b \leqslant x \leqslant L \tag{3.5}$$

At time $\Theta = 0$:

$$T_1(x, 0) = T_i \tag{3.6}$$

$$T_2(x, 0) = T_i \tag{3.7}$$

$$T_3(x, 0) = T_i \tag{3.8}$$

At $x = 0$:

$$Fo = -K_1 \left[\frac{\partial T_1}{\partial x} \right] \tag{3.9}$$

At x = a:

$$K_1 \left[\frac{\partial T_1}{\partial x}\right]_a = h_1(T_2-T_1) = K_2 \left[\frac{\partial T_2}{\partial x}\right]_a \tag{3.10}$$

At x = b:

$$K_2 \left[\frac{\partial T_2}{\partial x}\right]_b = h_2(T_3-T_2) = K_3 \left[\frac{\partial T_3}{\partial x}\right]_b \tag{3.11}$$

At x = L:

$$K_3 \left[\frac{\partial T_3}{\partial x}\right]_L = 0 \tag{3.12}$$

The contact conductance, h, is assumed to be independent of temperature and its values at the two interfaces are assumed to be equal, i.e. $h_1 = h_2$.

3.1.4 Finite Difference Approximation

The composite body is divided into eleven finite regions, with eleven nodal points to describe the temperature distribution. Figure 3.3 illustrates the model.

1st interface   2nd interface
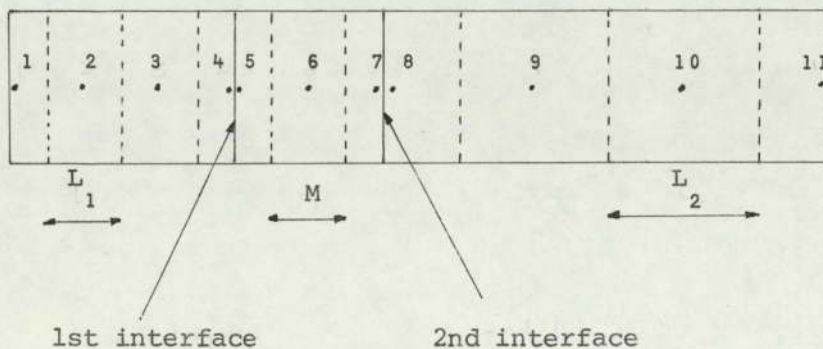
Figure 3.3

The length of each nodal divisions in the regions 1, 2 and 3 are

L_1, M and L_2 respectively.

Crank-Nicholson's finite difference scheme [19] is used to approximate the time-temperature history in the system. This is an implicit method, where the average of the finite difference approximation for $\partial^2 T/\partial x^2$ at time Θ and $\Theta + \Delta\Theta$ is used,

i.e.
$$\left[\frac{\partial^2 T}{\partial x^2}\right]_{\Theta + \frac{\Delta\Theta}{2}} = \frac{1}{2}\left[\left(\frac{\partial^2 T}{\partial x^2}\right)_{\Theta} + \left(\frac{\partial^2 T}{\partial x^2}\right)_{\Theta + \Delta\Theta}\right] \tag{3.13}$$

The finite difference approximation for $\partial^2 T/\partial x^2$ is:

$$\left(\frac{\partial^2 T}{\partial x^2}\right)_{n,\Theta} = \frac{T_{n+1,\Theta} - 2T_{n,\Theta} + T_{n-1,\Theta}}{\partial x^2} \tag{3.14}$$

and for $\partial T/\partial\Theta$ is:

$$\frac{\partial T}{\partial\Theta} = \frac{T_{n,\Theta + \Delta\Theta} - T_{n,\Theta}}{\Delta\Theta} \tag{3.15}$$

Hence, the one-dimensional heat conduction equation (3.2) in the finite difference form will be:

$$\frac{T_{n,\Theta + \Delta\Theta} - T_{n,\Theta}}{\Delta\Theta} + Q\left(T_{n,\Theta + \frac{\Delta\Theta}{2}} - T_i\right)^2 = \frac{\alpha}{2(\Delta x)^2}\left[(T_{n+1,\Theta} - \right.$$

$$2 T_{n,\Theta} + T_{n-1,\Theta}) + (T_{n+1,\Theta + \Delta\Theta} - 2 T_{n,\Theta + \Delta\Theta} +$$

$$\left. T_{n-1,\Theta + \Delta\Theta}\right] \tag{3.16}$$

Assuming

$$T_{n,\Theta + \frac{\Delta\Theta}{2}} = \frac{T_{n,\Theta + \Delta\Theta} + T_{n,\Theta}}{2} \tag{3.17}$$

Equation 3.16 becomes:

$$\Delta\Theta.T_{n,\Theta + \Delta\Theta} + 4 Z(n - 1).T_{n - 1,\Theta + \Delta\Theta} + (4 X(n) + Q.\Delta\Theta$$

$$(2 T_{n,\Theta} - 4 T_i)) T_{n,\Theta + \Delta\Theta} + 4 Y(n) T_{n + 1, \Theta + \Delta\Theta}$$

$$= 4 R(n) - Q.\Delta\Theta \left[T_{n,\Theta}^2 - 4 T_{n,\Theta}.T_i + 4 T_i^2 \right] \qquad (3.18)$$

in which the arrays X, Y, Z and R are defined in pages **30 - 32**

Hence, $T_{n,\Theta + \Delta\Theta}$ will depend on the temperature values at the adjacent nodal points at previous (Θ) and current ($\Theta + \Delta\Theta$) time steps. Equation 3.18 leads to eleven non-linear equations with eleven unknowns, $T_{n,\Theta + \Delta\Theta}$, n = 1 to 11. These equations were solved by Newton Raphson's iterative technique to evaluate the temperature profiles. The technique converges in two iterations. The equations, the method of solving them and the computer program written in Fortran IV for the evaluation are described in Appendix 2.

3.1.5 An Alternative Method

The eleven non-linear equations could be made linear with respect to $T_{n,\Theta + \Delta\Theta}$ if we introduce $T_{n,\Theta}$ instead of $T_{n,\Theta + \Delta\Theta/2}$ into the correction term in equation 3.16. Hence, these equations could be represented in matrix form AT = R, in which A is a tridiagonal matrix (11 x 11) and T and R are vectors. R contains known constant values and temperature values in the previous iterations $T_{n,\Theta}$. The assumption seems justified on comparing the temperature profiles obtained using either of these methods for a given heat flux F_o and contact conductance h_c values.

The nodal equations obtained using this assumption in the matrix form is:

$$
\begin{bmatrix}
X(1) & Y(1) & & & & \\
Z(1) & X(2) & Y(2) & & & \\
 & \ddots & \ddots & \ddots & & \\
 & & Z(9) & X(10) & Y(10) & \\
 & & & Z(10) & X(11) &
\end{bmatrix}
\times
\begin{bmatrix}
T_{1,\theta + \Delta\theta} \\
T_{2,\theta + \Delta\theta} \\
\vdots \\
T_{10,\theta + \Delta\theta} \\
T_{11,\theta + \Delta\theta}
\end{bmatrix}
=
\begin{bmatrix}
R(1) \\
R(2) \\
\vdots \\
R(10) \\
R(11)
\end{bmatrix}
\qquad (3.19)
$$

in which:

$$\text{For } I = 1 \text{ to } 3 \quad X(I) = 2 + 2\beta_1$$

$$X(4) = 2 + 2\beta_1 + 2\beta_1/N_1$$

$$X(5) = 2 + 2\beta_2 + 2\beta_2/N_2$$

$$X(6) = 2 + 2\beta_2$$

$$X(7) = 2 + 2\beta_2 + 2\beta_2/N_3$$

$$X(8) = 2 + 2\beta_3 + 2\beta_3/N_4$$

and for $I = 9$ to 11 $\quad X(I) = 2 + 2\beta_3$

$$Y(1) = -2\beta_1 \qquad\qquad Z(1) = -\beta_1$$

$$Y(2) = -\beta_1 \qquad\qquad Z(2) = -\beta_1$$

$$Y(3) = -\beta_1 \qquad\qquad Z(3) = -2\beta_1$$

$$Y(4) = -2\beta_1/N_1 \qquad Z(4) = -2\beta_2/N_2$$

$$Y(5) = -2\beta_2 \qquad\qquad Z(5) = -\beta_2$$

$$Y(6) = -\beta_2 \qquad\qquad Z(6) = -2\beta_2$$

$$Y(7) = -2\beta_2/N_3 \qquad Z(7) = -2\beta_3/N_4$$

$$Y(8) = -2\beta_3 \qquad Z(8) = -\beta_3$$

$$Y(9) = -\beta_3 \qquad Z(9) = -\beta_3$$

$$Y(10) = -\beta_3 \qquad Z(10) = -2\beta_3$$

and

$$R(1) = (2 - 2\beta_1) \cdot T_{1,\theta} + 2\beta_1 - T_{2,\theta} + \frac{2 F_o \cdot L_1}{K_1} - Q.\Delta\theta(T_{1,\theta} - T_i)^2$$

$$R(2) = \beta_1 \cdot T_{1,\theta} + (2 - 2\beta_1) \cdot T_{2,\theta} + \beta_1 \cdot T_{3,\theta} - Q.\Delta\theta.(T_{2,\theta} - T_i)^2$$

$$R(3) = \beta_1 \cdot T_{2,\theta} + (2 - 2\beta_1) \cdot T_{3,\theta} + \beta_1 \cdot T_{4,\theta} - Q.\Delta\theta.(T_{3,\theta} - T_i)^2$$

$$R(4) = 2\beta_1 \cdot T_{3,\theta} + (2 - 2\beta_1 - 2\beta_1/N_1) T_{4,\theta} + (2\beta_1/N_1) T_{5,\theta} - Q.\Delta\theta.(T_{4,\theta} - T_i)^2$$

$$R(5) = (2\beta_2/N_2) \cdot T_{4,\theta} + (2 - 2\beta_2 - 2\beta_2/N_2) \cdot T_{5,\theta} + 2\beta_2 T_{6,\theta} - Q.\Delta\theta.(T_{5,\theta} - T_i)^2$$

$$R(6) = \beta_2 \cdot T_{5,\theta} + (2 - 2\beta_2) T_{6,\theta} + \beta_2 \cdot T_{7,\theta} - Q.\Delta\theta.(T_{6,\theta} - T_i)^2$$

$$R(7) = 2\beta_2 \cdot T_{6,\theta} + (2 - 2\beta_2 - 2\beta_2/N_3) \cdot T_{7,\theta} + (2\beta_2/N_3) \cdot T_{8,\theta} - Q.\Delta\theta.(T_{7,\theta} - T_i)^2$$

$$R(8) = (2\beta_3/N_4) T_{7,\theta} + (2 - 2\beta_3 - 2\beta_3/N_4) \cdot T_{8,\theta} + 2\beta_3 \cdot T_{9,\theta} - Q.\Delta\theta.(T_{8,\theta} - T_i)^2$$

$$R(9) = \beta_3 \cdot T_{8,\theta} + (2 - 2\beta_3) \cdot T_{9,\theta} + \beta_3 \cdot T_{10,\theta} - Q.\Delta\theta.(T_{9,\theta} - T_i)^2$$

$$R(10) = \beta_3 \cdot T_{9,\theta} + (2 - 2\beta_3) \cdot T_{10,\theta} + \beta_3 \cdot T_{11,\theta} - Q.\Delta\theta.(T_{10,\theta} - T_i)^2$$

$$R(11) = 2\beta_3 T_{10,\theta} + (2 - 2\beta_3) \cdot T_{11,\theta} - Q.\Delta\theta.(T_{11,\theta} - T_i)^2$$

in which

$$\beta_1 = \frac{\alpha_1 \cdot \Delta\theta}{L_1^2}$$

$$\beta_2 = \frac{\alpha_2 \cdot \Delta\Theta}{M^2}$$

$$\beta_3 = \frac{\alpha_3 \cdot \Delta\Theta}{L_2^2}$$

$$N_1 = \frac{K_1}{h_c \cdot L_1}$$

$$N_2 = N_3 = \frac{K_2}{h_c \cdot M}$$

$$N_4 = \frac{K_3}{h_c \cdot L_2}$$

A computer programme written in Fortran IV to evaluate the temperature profiles using Gauss-Jordon's elimination technique [19] is given in Appendix 3. Appendix 3 also includes the comparison of the temperature profiles predicted by the two methods.

3.1.6 Dimensionless Analysis

The differential equations (3.3 to 3.5) and their boundary conditions contain a considerable number of experimental variables (Θ, T, x, h etc) and thermophysical properties (α, c, ρ etc). So as to display the interrelation of these quantities, and hence to help the interpretation of experimental time-temperature curves, the equations have been expressed in the dimensionless form. Three dimensionless groups were obtained by writing in dimensionless form, the equation and the boundary conditions.

This leads us to the following dimensionless groups on which the solution to the system will depend.

1. Dimensionless temperature = $K.T/(F_o.L)$
2. Dimensionless time = $\alpha.\Theta/L^2$
3. Dimensionless contact conductance = $h_c L/K$

DIM.TIME X.10⁻³
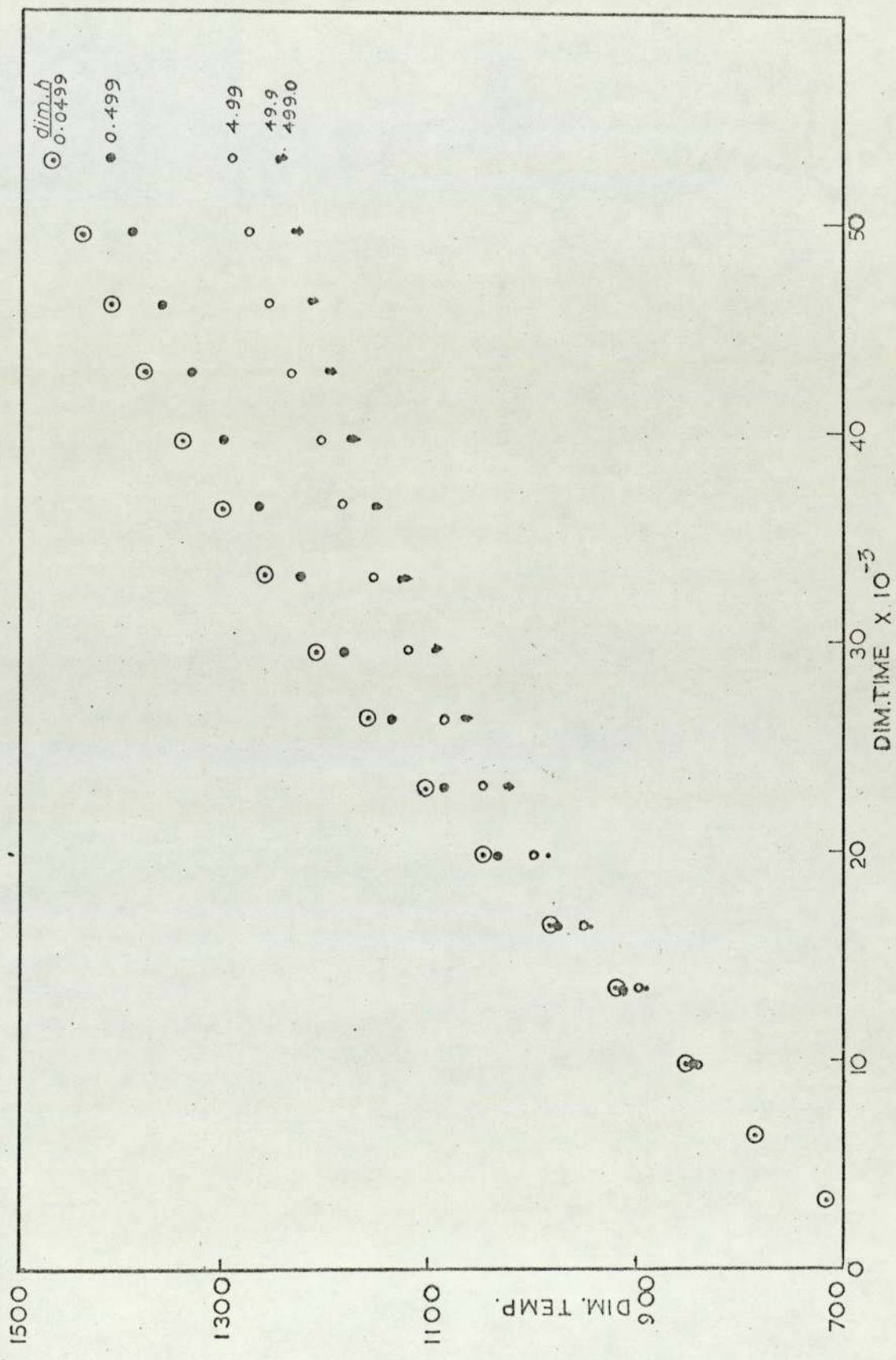
Figure 3.4

The groups chosen with appropriate parameters for the interpretation are:

$$\text{Dimensionless temperature} = (K_1 . T_{2,\theta})/F_o . d \qquad (3.20)$$

$$\text{Dimensionless time} = \alpha_1 . \theta/d^2 \qquad (3.21)$$

$$\text{Dimensionless contact conductance} = h_c d/K_1 \qquad (3.22)$$

in which α_1 is the thermal diffusivity of the material in region 1 (Figure 3.1), d is the thickness of the plastic material and other quantities are defined before.

From the theoretically predicted temperature profiles using the computer program given in Appendix 3, a family of curves of dimensionless temperature against dimensionless time can be plotted for given values of F_o and the initial temperature distribution. The curves obtained were found to take the shapes as shown in Figure 3.4. These curves suggest the limits to the accuracy with which the experimental method can measure thermal contact conductance, h.

Figure 3.4 also suggests that conductance values greater than $\sim$ 500 BTU/hr ft^2 ^{o}F (Dim.h 49.9) will be indistinguishable, since the curves corresponding to conductance values in this range of values lie closely together. At lower values of conductance h_c the accuracy will be limited by:

(i)   the accuracy of the temperature measurements

(ii) the agreement of the experimental temperature profile with the general shape of the graph.

If the circular points in Figure 3.5 represent a set of experimental points and the continuous lines represent a plot of dimensionless
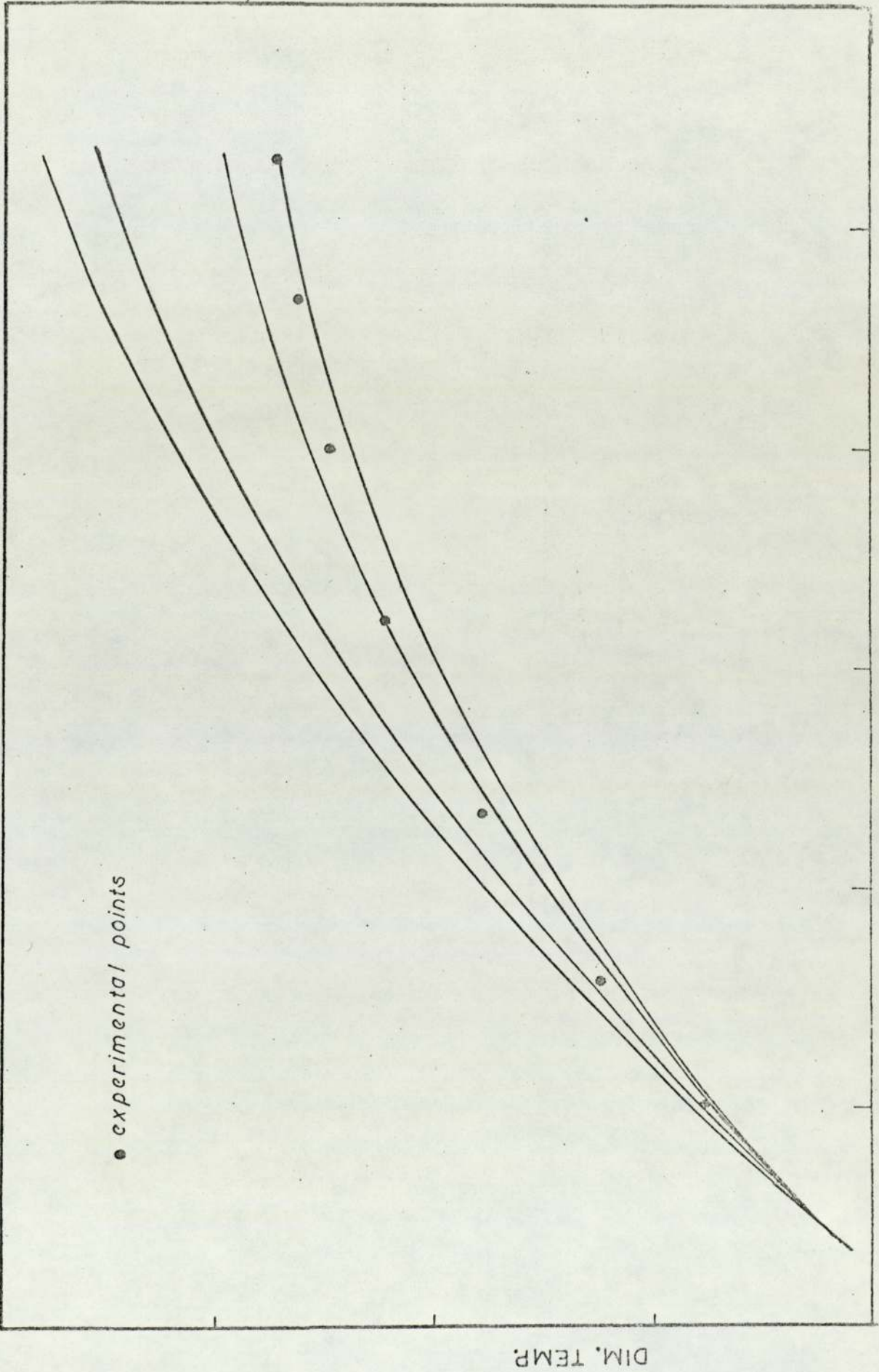
DIM. TIME
Figure 3.5

time against dimensionless temperature obtained theoretically using
the corresponding experimental condictions, then it will be only
possible to predict a range for the conductance values from a
particular experimental data. For the assumptions made in building
up the mathematical model to be valid, the general shape of the
experimental profiles should be the same as that obtained
theoretically. The relationship will be a guide for the analysis
of the experimental data.

3.2 <u>A Transient Method of Measuring Heat Flux at $x = o$ (F_o)</u>

The transient temperature profiles set up in the composite
rod is caused by the heat flux, F_o, radiated from a high temperature
furnace. Analysis of the temperature-time profiles requires a
knowledge of the value of F_o. In order to measure this heat flux
at $x = o$ (Figure 3.1) when it is exposed to the radiant heat source,
F_o is assumed to be constant during the process of transient heating.
The absolute temperature at $x = o$ will be small compared to that
of the furnace. If the furnace temperature and the emissivity of
the surface $x = o$ are kept constant, the change of F_o due to the
change of temperature at $x = o$ during the process is illustrated
in Table 3.1. The table includes the range of furnace temperatures
and surface temperatures in which the experiments were carried
out.

FURNACE TEMP. $^\circ R$ T_F	SURFACE TEMP. $^\circ R$ T_S	PERCENTAGE CHANGE OF F_o i.e. $(T_F^4 - T_S^4)$
2000	550	0.000
2000	575	0.125
2000	600	0.250
2000	625	0.375
2000	650	0.5825
2400	550	0.000
2400	575	0.0625
2400	600	0.125
2400	625	0.1875
2400	650	0.291

Table 3.1

The experimental method of measuring heat flux at x = o uses a short
rod insulated at one end and edge of whose exposed end is identical
in area and surface emissivity to the rod of the main transient
experiments.
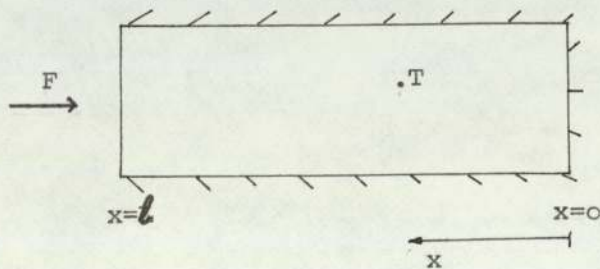
Figure 3.6

The temperature at any point x on the rod at time Θ is:

$$T = \frac{F_o.\Theta}{\rho.c.1} + \frac{F_o.1}{K} \left[\frac{3x^2 - 1^2}{1^2} - \frac{2}{\pi^2} \sum_{n=1}^{\infty} \frac{(-1)^n}{n^2} e^{\frac{-\alpha_n^2\pi^2\Theta}{1^2}} \cos \frac{n\pi x}{1} \right]$$

(3.23)

in which the slab at zero initial temperature receives a constant

heat flux, F_o at x = 1 and there is no flow of heat across at

x = o [2] (Figure 3.6).

The temperature distribution corresponds to a linear increase

with time $F_o.\Theta/\rho.c.1$. together with a correction term which depends

on x, the position, the time Θ and the length of the slab 1. Hence:

$$T = \frac{F_o.\Theta}{\rho.c.1} + \text{correction term}$$

(3.24)

The correction term was found small when compared to the main term,

$F_o\Theta/\rho.c.1$ for x/1 in the range of 1/3 to 2/3 and for small 1.

Table 3.2 gives the values of the main terms and the corresponding

correction terms for

$$F_o = 2000 \quad \text{BTU/hr ft } ^oF$$

$$1 = 0.25 \quad \text{ft}$$

$$x/1 = 1/3, 1/2, 2/3$$

$$\rho = 169.0 \quad \text{lb/ft}^3$$

$$c = 0.213 \quad \text{BTU/lb } ^oF$$

$$\Theta = 1/2 \quad \text{hr}$$

x/1	MAIN TERM $\frac{F_o.\Theta}{\rho.c.1}$	CORRECTION TERM
1/3	168.014	-0.5439
1/2	168.014	-0.2039
2/3	168.014	+0.2723

Table 3.2

Hence, the heat flux could be measured with the assumption that the temperature T, increases linearly with time in the range of values of x/l and Θ given in Table 3.2 when one end receives a constant heat flux.

If the initial temperature of the rod is T_i, then:

$$T = T_i + \frac{F_o \cdot \Theta}{\rho . c . l} \qquad (3.25)$$

i.e. $\qquad F_o = \rho . c . l \frac{dT}{d\Theta} \qquad (3.26)$

$dT/d\Theta$ will be obtained from the thermal transients produced by the heat flux F_o in a rod of length l, density ρ and specific heat c.

3.3 Least Squares Procedure for Comparison of Theory and Experiment

The technique used in this study finds the thermal contact conductance (h_c) between metal and plastic surfaces and the thermal conductivity of the plastic material (K_p) by comparing the temperature-time variation predicted by equations 3.3 to 3.12 (a variation that depends on h_c and K_p) with the temperature-time variation found by experiment. The values of contact conductance and the conductivity of the plastic material are those which give the closest agreement between predicted and measured temperatures.

The sum of squares function F, for n thermocouples at m discrete time steps

$$F(h_c, K_p) = \sum_{j=1}^{m} \sum_{i=1}^{n} \left[Tc_{i,j}(h_c, K_p) - T_{E_{i,j}} \right]^2 \qquad (3.27)$$

has to be minimised with respect to h_c and K_p

in which Tc = predicted temperature

T_E = measured temperature

Optimisation techniques were used to find the minimum of this function. The spiral algorithm[32] was used for this purpose. The flowchart for the proposed experimental procedure to estimate these parameters is given in Figure 3.7.

INPUT
1. Physical properties
   of test pieces
2. Eqns, initial and
   boundary conditions

INPUT
I.Known heat flux

THE
MATHEMATICAL
MODEL

THE
EXPERIMENTAL
EQUIPMENT

THEORETICAL
TEMPERATURE T_C
FOR GIVEN VALUES
OF VARIABLES

EXPERIMENTAL
TEMPERATURE T_E

NEW VALUES OF
VARIABLES
TOWARDS THE
MINIMUM POINT

CALCULATION OF
LEAST SQUARE
FUNCTION

OPTIMIZATION
TECHNIQUE TO
FIND OUT THE
MINIMUM OF FN.

REACHED
MININUM
POINT?

NO

YES

WRITE THE VALUES OF
VARIABLES AT MINIMUM
POINT

Figure 3.7

S E C T I O N   4

EXPERIMENTAL

The aim of this section was to provide temperature-time curves, which together with the theoretically predicted temperature values formed the sum of squares function. The data required was the temperature transients set up in two aluminium alloy rods which sandwich between them a thin sheet of plastic material, when one end of the rod receives a known constant radiant heat flux. This section briefly describes the design, construction and operation of the apparatus used for these measurements.

The apparatus was used to measure two quantities. Firstly to obtain the thermal transients produced by a constant heat flux on the composite rod and secondly the thermal transients set up in a 1" diameter and 3" long aluminium alloy rod by a constant radiant heat flux which enabled us to evaluate the heat flux provided by the high temperature furnace.

4.1 Apparatus

The apparatus consisted mainly of three parts, a high temperature furnace, a test chamber containing the composite rod and a pressure chamber (Figure 4.1).

The high temperature furnace (Griffin electric furnace 250 V, 12 Amp) provided a constant radiant heat flux. It can be heated up to a maximum temperature of 1200°C. The maximum temperature can be varied by means of an energy regulator. The furnace has a sliding door 8" x 6" and a heat shield was fixed between this door and the Test Chamber. The shield was made of aluminium sheet, lined with aluminium foil, in the form of a
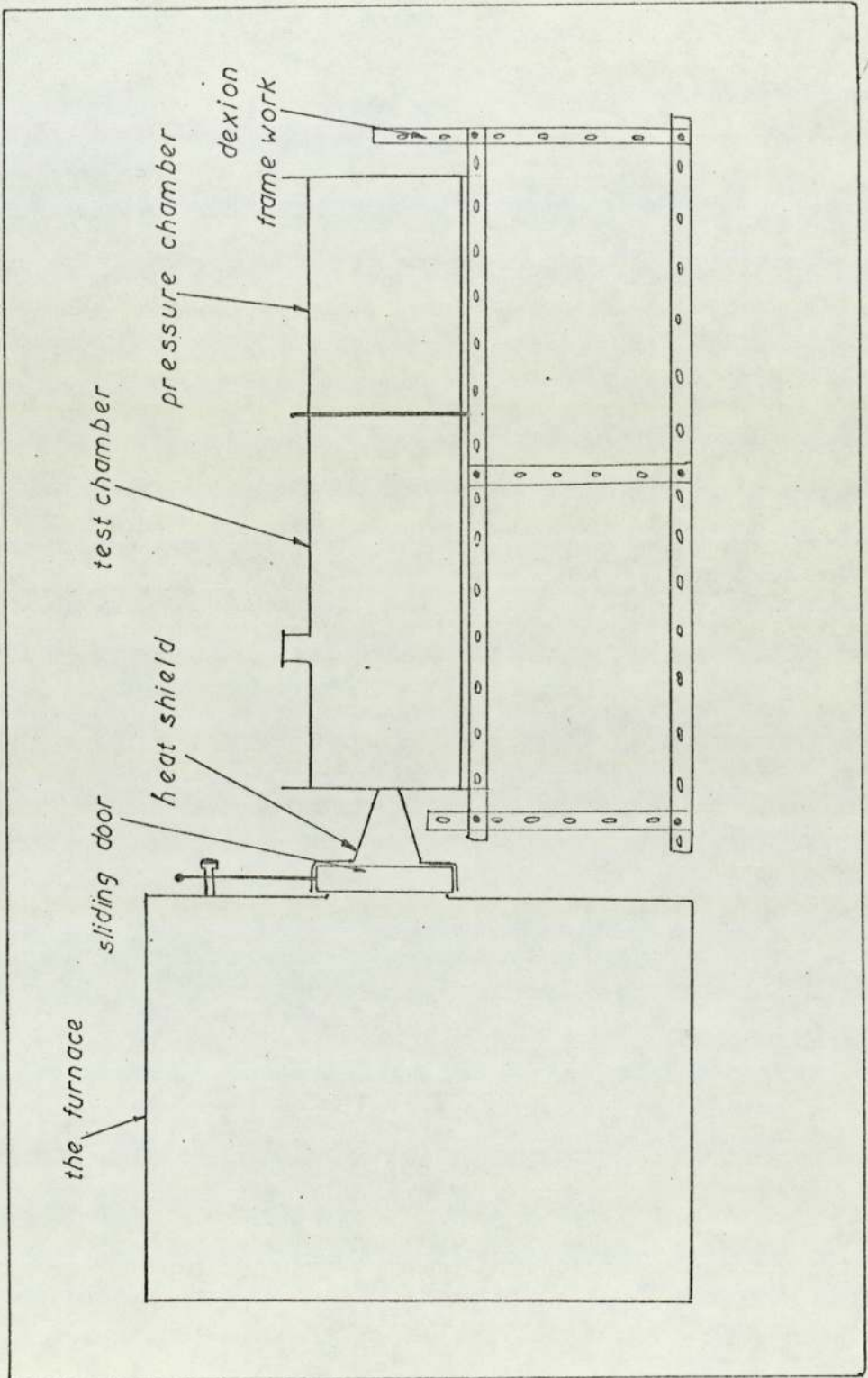
Figure 4.1. Apparatus for Contact Conductance Measurement

hollow truncated cone, 2.5" and 1.5" diameter at the ends and 4" in height. The purpose of this shield was to reduce heat loss from the furnace by convection to maintain a constant furnace temperature.

The test chamber was made of a mild steel pipe, 5.25" internal diameter, 0.25" thickness and 18" long. Two flanges each 8" x 8" were welded to the ends of the pipe. To one of these flanges was clamped an aluminium disc 8" diameter.

An IR radiation window ('vitriosil O66' silica glass), 6 cm diameter was fitted at the centre of this disc. The thickness of the glass window was 1 cm which would stand a pressure difference of one atmosphere. This glass would pass radiant energy. Figure 4.2 shows schemetrically the arrangement of the composite rod in the test chamber.

The pressure chamber was also made of mild steel pipe of the same diameter as the test chamber but 14" long. A flange 8" x 8" was welded to one end of the pressure chamber while the other end was closed with a steel plate 8" x 8" welded across the pipe. An aluminium disc 8" diameter and a flexible diaphram of the same diameter were sandwiched between the test chamber. The central part of this disc was machined in the form of a socket, such that a cylinder 3.5" diameter and 1" thick can smoothly slide in it. One end of the longer metal test specimen was clamped to this cylinder, while the other end was supported by means of a 'spider'. The socket and cylinder arrangement is illustrated in Figure 4.2. The flexible diaphram was an 0.1" thick rubber sheet. The two chambers and the diaphram allow independent adjustment of the ambient and applied pressures.

pressure chamber

flexible diaphragm

socket and
cylinder arrangement

test chamber

spider to hold
test specimen

insulation

metal
rods

glass window

plastic material

radiation
window

heat shield
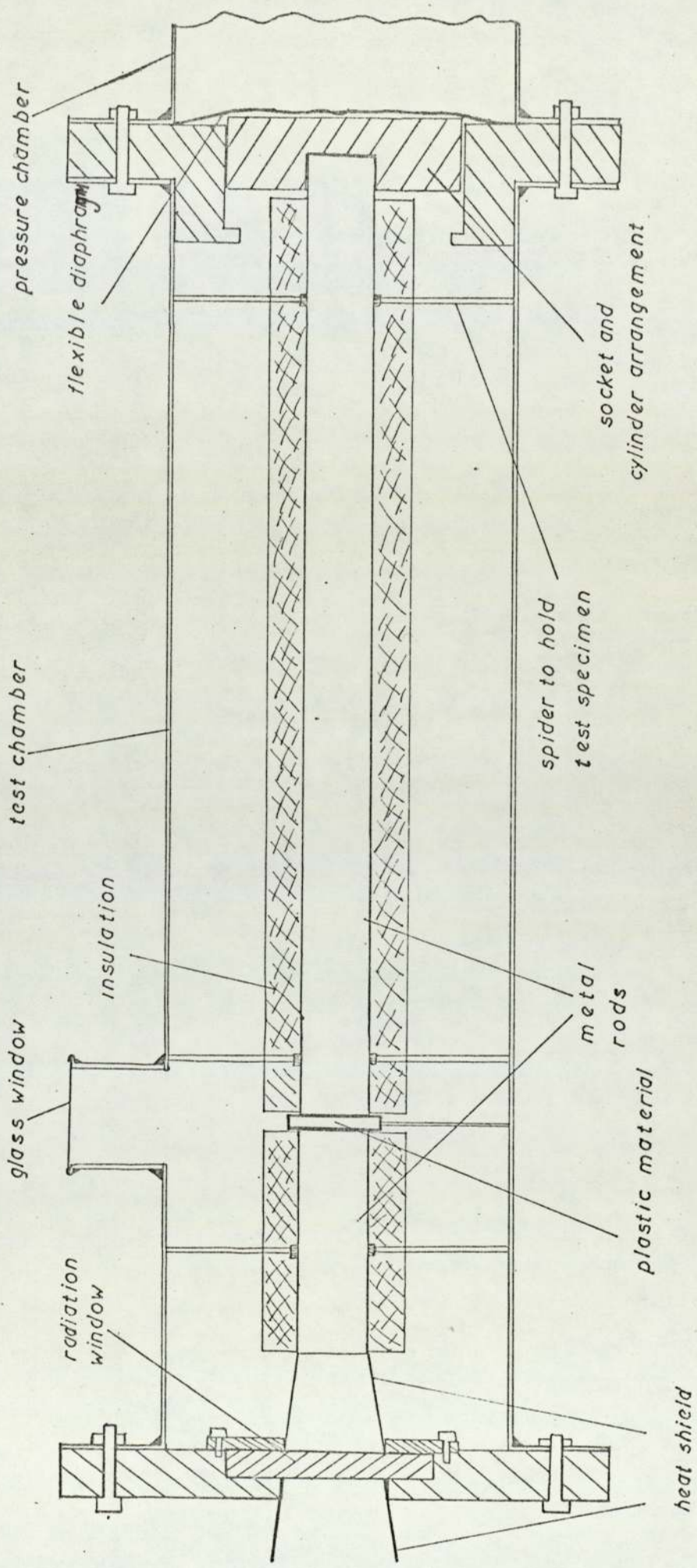
Figure 4.2   The Test Chamber
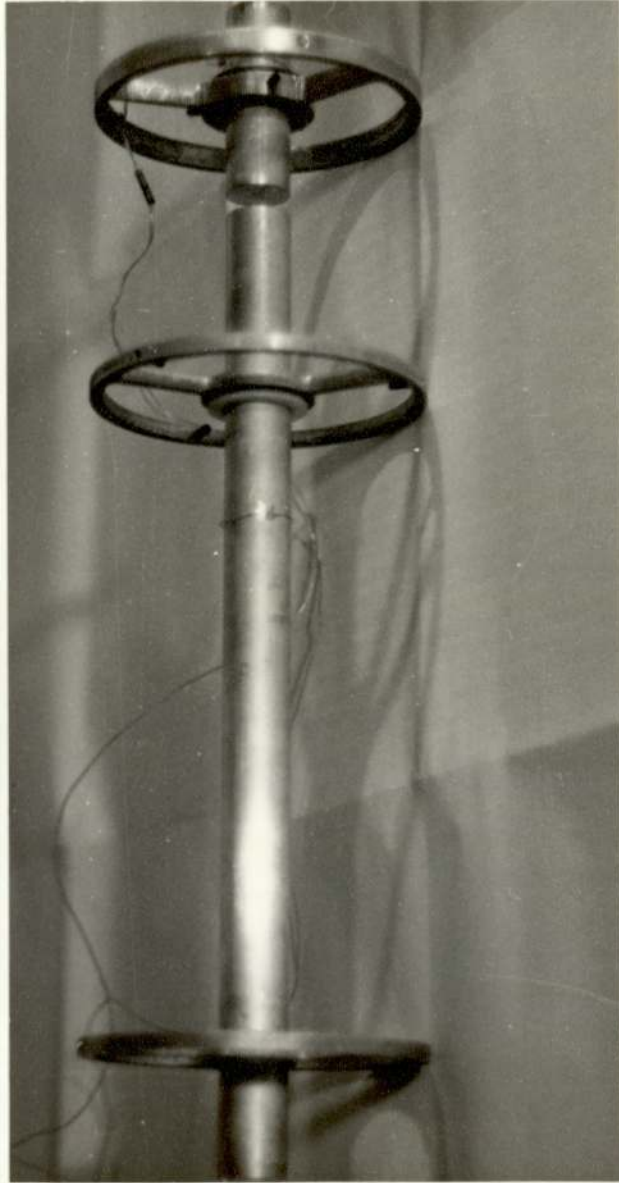
A View of the Metal Specimens and 'Spiders'

Figure 4.3
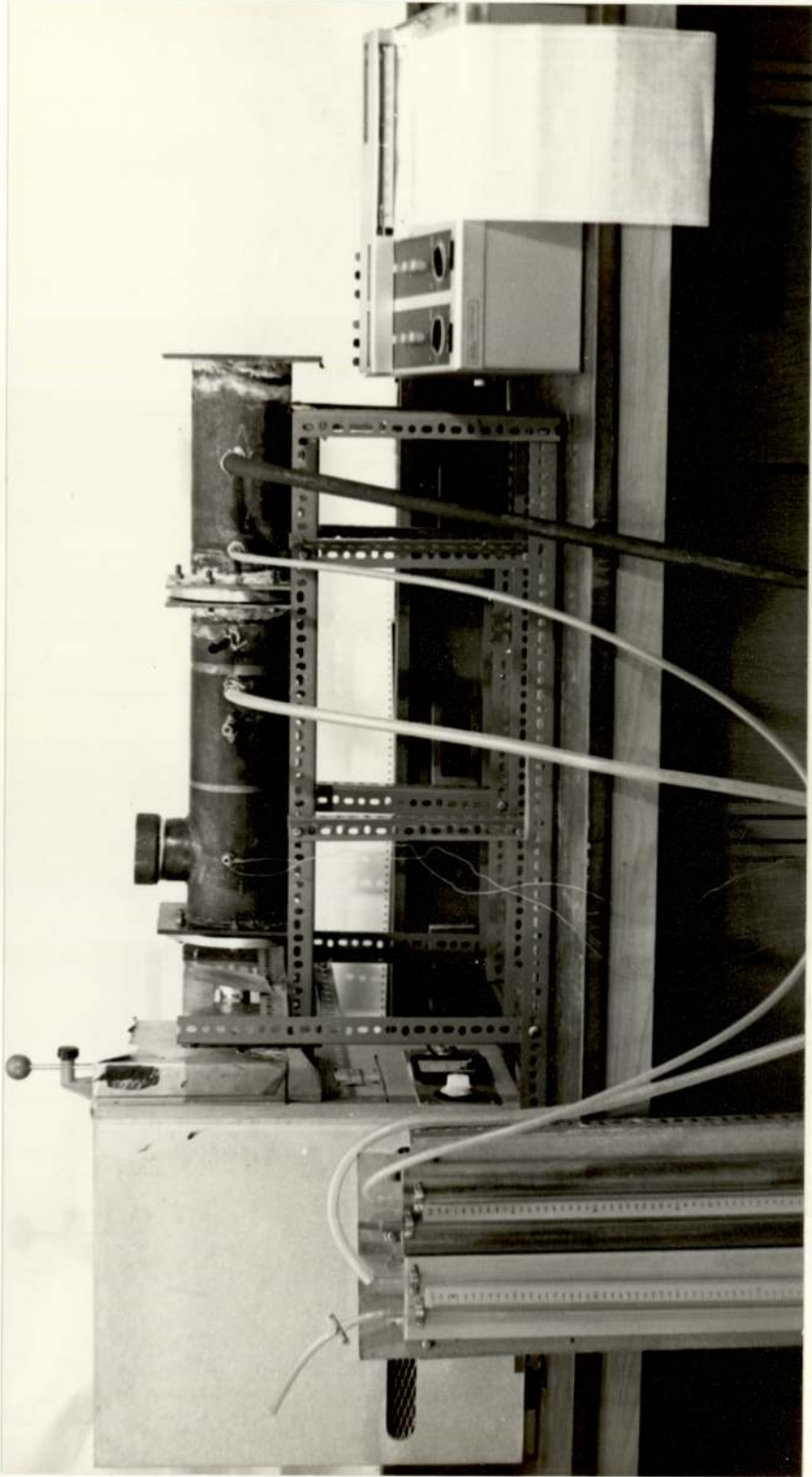
Photograph of the Apparatus

Figure 4.4

The smaller rod 3" long was supported by a 'spider' closer to the radiation window. The plastic material in the form of a disc 1.5" diameter and 1/16" thick was clamped to a 'spider' and sandwiched between the two metal rods. The photograph in Figure 4.3 provides a view of the metal specimens and 'spiders'. The spiders provided good alignment of the test specimens.

The test chamber and the pressure chamber clamped together were supported in a dexion framework (Figure 4.4). The test chamber was connected to a mercury manometer and to a vacuum pump by means of 'simplifix' couplings and pressure tubings. The pressure chamber was connected in a similar manner to mercury manometer and to the exhaust outlet of the vacuum pump. The pump used was an Edwards, ISC 30 series and single stage. It is capable of supplying compressed air through the exhaust outlet at 10 lb/in^2 continuously and 20 lb/in^2 intermittently.

The temperature measurements were made using alumel-chromel thermocouples and a servoscribe 2, RE 520.20, potentio-metric recorder. The recorder can be easily calibrated. It was calibrated for a full chart scale of 4.1 mv which is equivalent to $100^{\circ}C$ for a standard alumel-chromel thermocouple.

Test Specimen

The metal test specimens were constructed from 1" diameter HE 30 WP aluminium alloy rods. The length of the smaller rod was 3". One thermocouple was located on this rod 1" from the end closer to the radiation window. This end was painted black using a mixture of carbon black and sodium silicate. The length of the other metal specimen was 14.25" and a thermocouple was located at

4.75" from the end which is in contact with the plastic material
(Figure 4.2). The plastic material used was 'Tyril' (Styrene
acrylonitrile copolymer) obtained in the form of pellets. These
were moulded in the form of discs 1.5" diameter and 1/16" thickness.
The surface roughness of the metal samples were measured in the
Production Engineering laboratory. Since our experimental program
did not include the effect of surface roughness on contact conduc-
tance, the roughness of the metal surfaces in contact was kept
constant. The plastic specimens were moulded in the same mould
from the same bulk of pellets to ensure uniformity and equal
surface roughness. The location of thermocouples in the metal
specimen corresponds to the nodal points 2 and 9 in the model
given in Figure 3.2. 3

The thermocouples were installed in slots rather than in
drilled holes. This type of installation was reported by Watson
and Robinson [31] National Bureau of Standards. The specimens used
for his work were 2.54 cm diameter rods and the welded junctions
were peened into holes 0.11 cm diameter and 0.17 cm deep. The
installation of thermocouples for the present work, was based on
the techniques of Moore [6] . The alumel and chromel wires used
were 0.0148" diameter. The measuring junctions were formed by butt
welding. Good welding was achieved after some experimentation.
It provided a fairly uniform junction. These junctions were
embedded in narrow slots cut tangentially on the surface of the
rods at required locations, (Figure 4.5). The edges of the slots
were folded over the wire to ensure the safety of the wires and to
achieve good contact between the junction and the specimen. The
wires insulated with P.V.C. sleeves were wrapped around the sample.
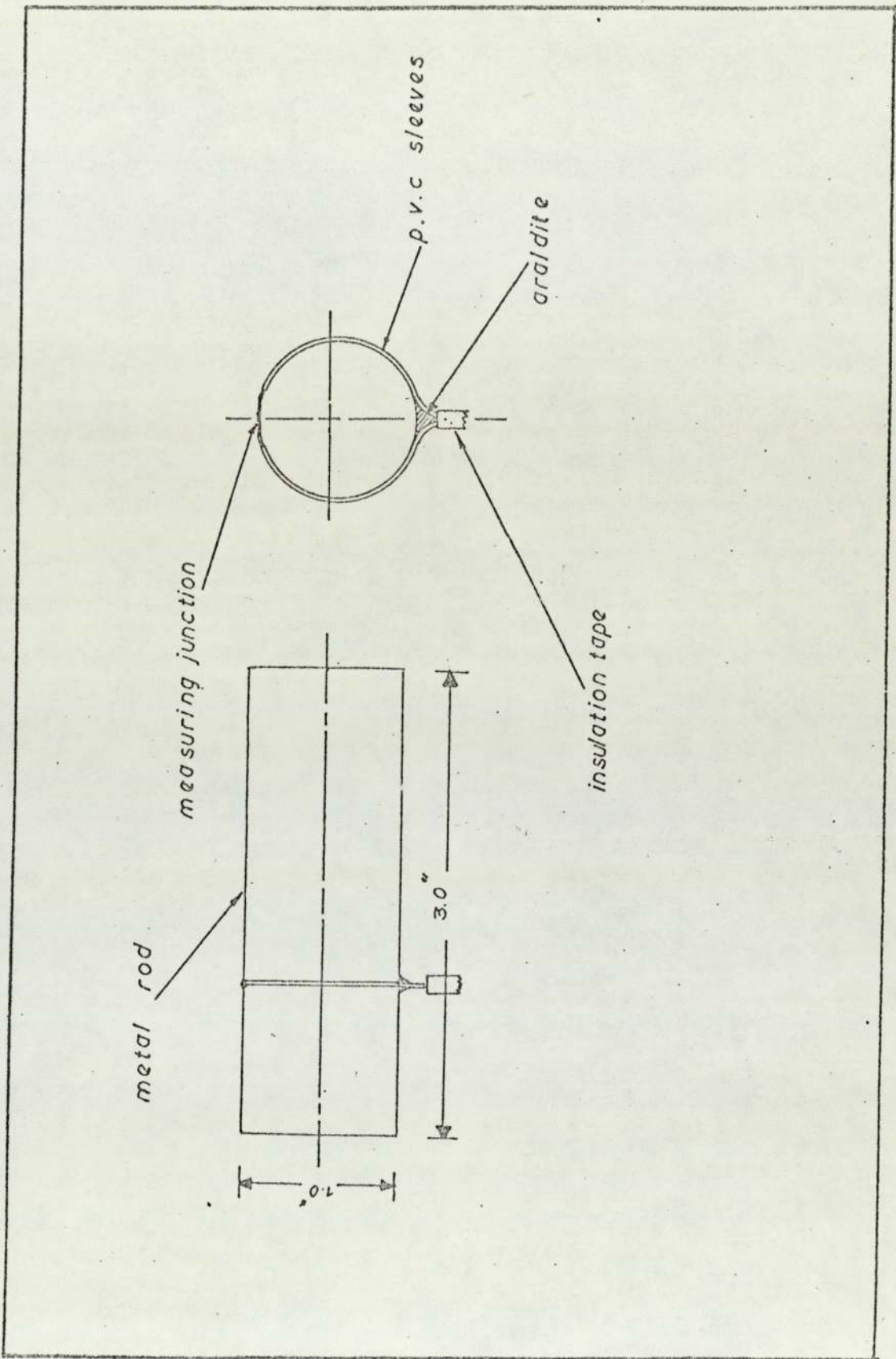
Figure 4.5   Thermocouple Location Details

At the point where the wires meet on the opposite side of the slot, the wires were wrapped together by a piece of insulation tape. The upper portion of the tape was pasted on to the rod using araldite to prevent relative motion between the wires and the rod. The test specimens were held in melting ice and boiling water to calibrate the thermocouples. The reference junctions were always kept in melting ice during the temperature measurements. The e.m.f. produced at these two temperatures agree with the data for a standard alumel-chromel thermocouple.

4.2 Experimental Procedure

The furnace with heat shield fitted (Figure 4.1) was switched on with the door closed. When the temperature reached about $1000^{\circ}C$, the furnace door was opened with a square sheet of aluminium 4" x 4" painted black with carbon black and sodium silicate mixture placed across the heat shield. As the temperature of the furnace reached a steady state under these conditions, the furnace was ready to provide a constant heat flux. An average time of 30 minutes was taken for the furnace to reach this steady temperature after opening the door. The aluminium sheet 4" x 4" was painted black in order to match the emissivity of the surface of the rod at $x = o$, to maintain a constant furnace temperature.

4.2.1 Measurement of Heat Flux, F_o

The experimental set-up for the measurement of heat flux is given in Figure 4.6. The aim was to obtain the thermal transients set up in a 3" long metal rod when the end receives a constant heat flux. A thermocouple was installed 1" from the
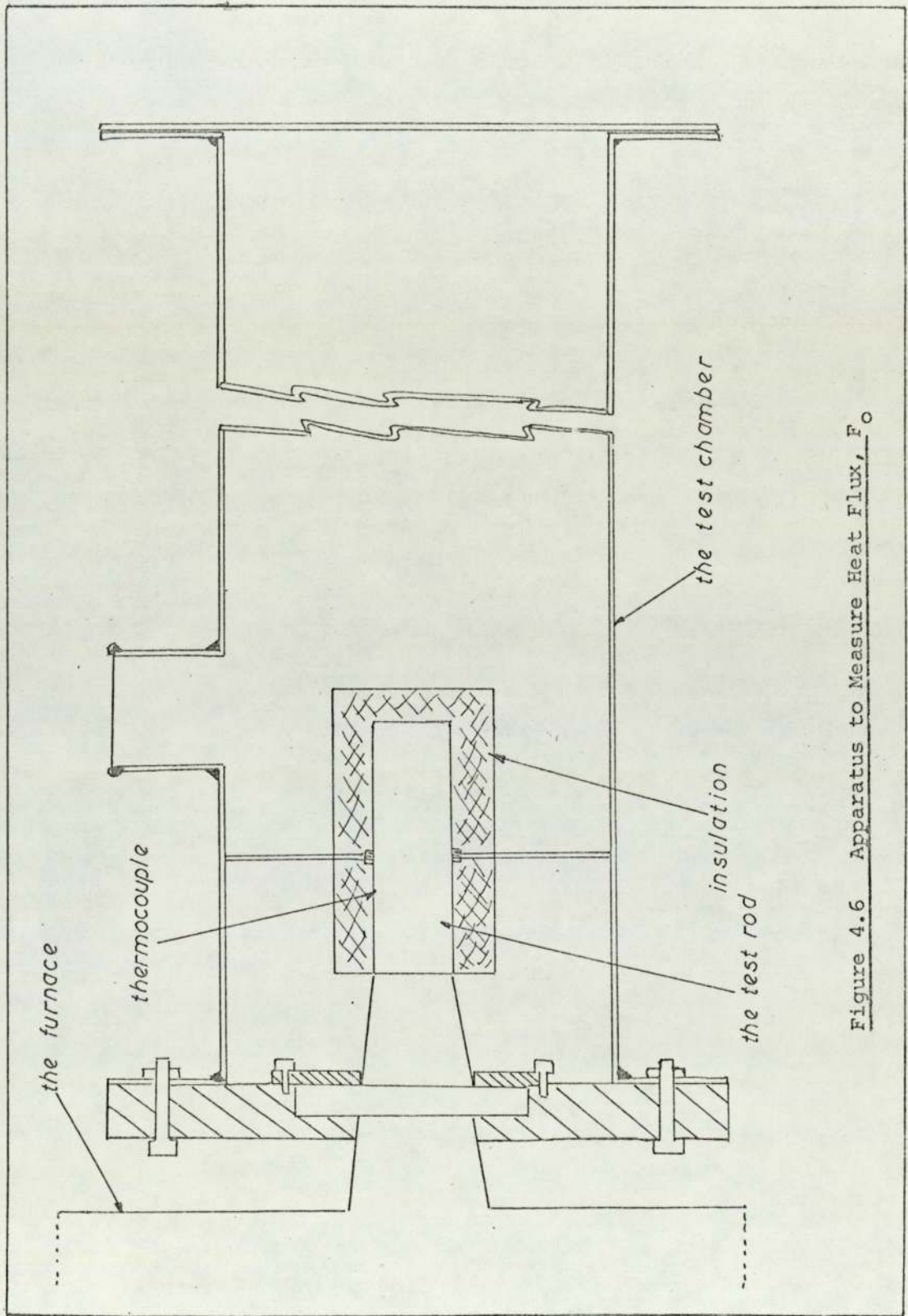
Figure 4.6   Apparatus to Measure Heat Flux, F_o

the test chamber

insulation

the test rod

thermocouple

the furnace

heated end. The flat surface of the end of the rod closer to the thermocouple was painted black with a mixture of carbon black and sodium silicate solution. The rod was insulated first with a layer of asbestos and outside of this with 1" thick foamed polyurethane. The rod was fitted onto a spider and placed in the test chamber with the end painted black towards the radiation window. The spider was clamped to the inside of the test chamber by means of allen screws. Between the radiation window and the end of the rod was another heat shield to prevent heat loss by convection from the end of the rod. The thermocouple wires were connected to the recorder with the reference junction in melting ice. The aluminium disc with radiation window was then clamped to the flange.

The square sheet of aluminium was removed and the test chamber was brought into position immediately such that the end of the rod received the heat flux through the radiation window. The potentiometric recorder produced e.m.f. data which enabled us to obtain the rate of increase of temperature on the rod.

At the end of 30 minutes, the test chamber was removed from the heat flux and the square sheet of aluminium was brought back as before across the heat shield. The rate of decrease of temperature in the rod was then recorded for 60 minutes. This data enabled us to obtain the surface heat loss during the transient heating (first 30 minutes of the experiment).

In agreement with the equation (3.23),

i.e. $$T = T_i + \frac{F_o}{\rho.c.l.} \cdot \theta$$

the plot of T against θ was found to be a straight line when T was corrected for the heat loss. Figure 4.7 is a graph of T
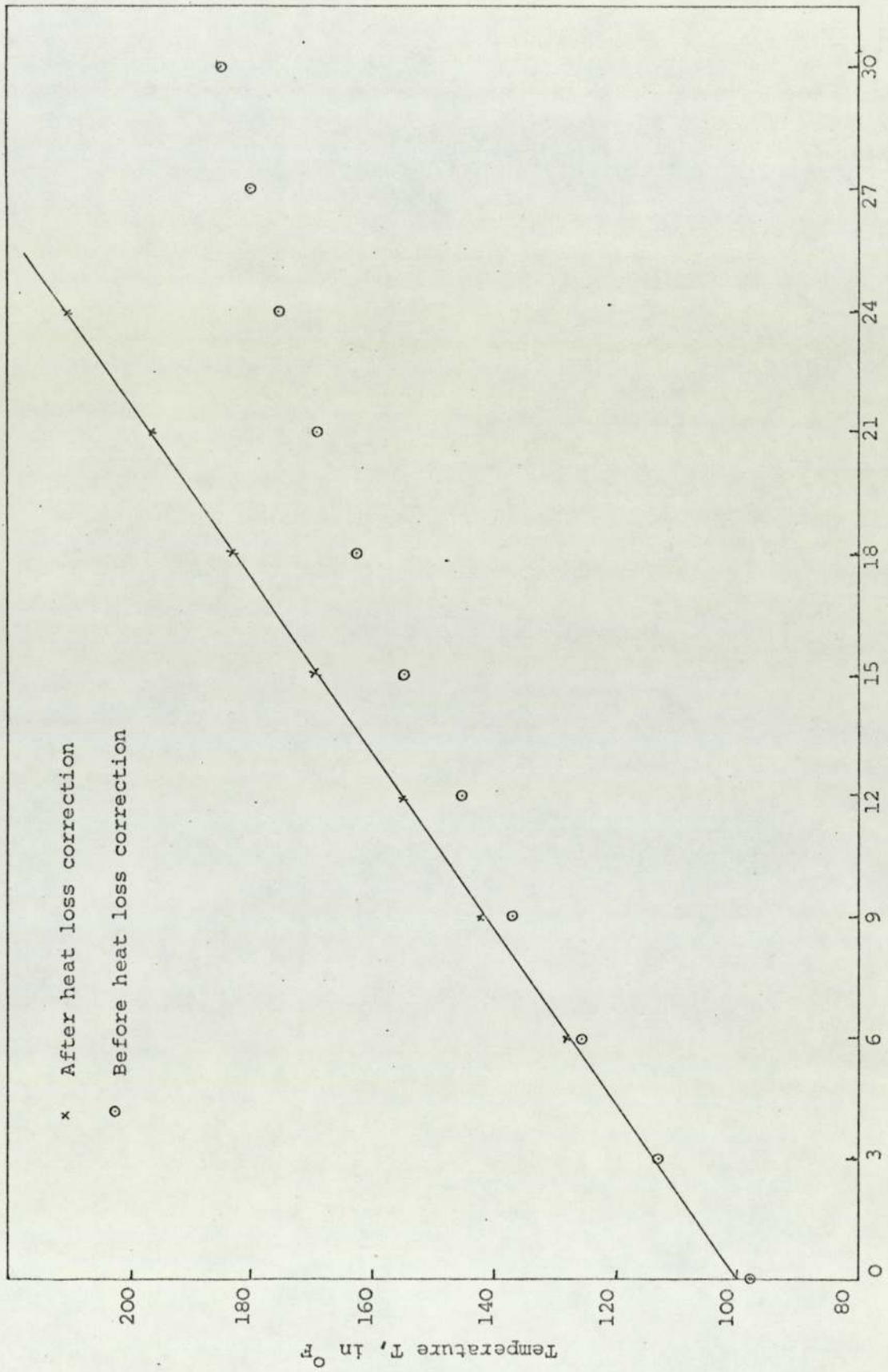
Figure 4.7   The General Shape of T vs. θ graph

against θ obtained from experimental data before and after heat
loss correction. Hence, the heat flux received by the end of
the rod from the furnace was obtained from equation (3.24)

i.e. $$F_o = \rho.c.l. \frac{dT}{d\theta}$$

in which $\frac{dT}{d\theta}$ = slope of T vs θ after the heat loss correction

$\quad\quad\quad$ ρ = density of the rod

$\quad\quad\quad$ c = specific heat of the rod

$\quad\quad\quad$ l = length of the rod.

For the experimental system:

$\quad\quad\quad$ ρ = 169.0 lb/ft^3

$\quad\quad\quad$ c = 0.213 BTU/lb ^{o}F

$\quad\quad\quad$ l = 0.25 ft

The rate of decrease of temperature was assumed to be only due
to the surface loss. The effect of the axial flow of heat
during cooling on the rate of decrease of temperature on the
rod will be negligible (Appendix 1). The fluctuation in the
furnace temperature was less than 3^oC. Hence, the heat flux
provided by the furnace was regarded as constant throughout the
experiment.

4.2.2 Measurement of Thermal Transients in the Composite Rod

$\quad\quad$ The aim of the experimental work was to obtain the thermal
transients set up in the composite system (Figure 4.2) when the
end of the smaller rod receives a previously measured constant
heat flux. The experimental program included the investigation
of:

(i) the effect of applied pressure

(ii) the effect of ambient pressure

on contact conductance. The following section describes the
experimental technique involved in these measurements.

Program (i)

The effect of applied pressure was obtained when the
specimens were at atmospheric pressure. The test pieces were
arranged in the test chamber as shown in Figure 4.2. Initially
the longer rod, well insulated, was introduced and then the
plastic material and the smaller rod. The spiders attached to
the longer rod can slide along the wall of the test chamber,
while that of the smaller rod was clamped to the wall at the
same position as before in the heat flux measurement experiment.
This was to ensure that the end of the smaller rod receives the
same heat flux that was already measured.

In order to apply pressure against the contact, the
exhaust outlet of the vacuum pump was connected to the pressure
chamber while the suction side of the pump was exposed to the
atmosphere. The pressure chamber was connected to a manometer
by means of a 'simplifix' coupling and pressure tubing. The
cold junctions of the thermocouples were kept in melting ice.
Firstly the pressure was applied against the contact by increasing
the pressure inside the pressure chamber. When the required
ambient pressure was reached inside the pressure chamber, the
valve between the pressure chamber and the pump was switched
off. If the ambient pressure inside the test chamber is p_1 and
that in the pressure chamber is p_2:

the pressure across the diaphram   = $(p_2 - p_1)$

hence, the pressure across the contact   = $(p_2 - p_1) \dfrac{A^2}{a^2}$ (4.1)

in which A and a are the diameters of the aluminium cylinder and of the rod respectively (Figure 4.8).

The diameter of the cylinder   A = 3.5"

and the diameter of the rod   a = 1.0"

hence, the contact pressure = 12.25 $(p_2 - p_1)$ for $(p_2 > p_1)$

(4.2)

The square aluminium sheet was removed and the end of the smaller rod in the composite system was allowed to receive the heat flux. The thermal transients set up in the aluminium rods were recorded for 30 minutes.

Program (ii)

The test specimens were arranged as in program (i). The exhaust outlet of the pump was disconnected from the pressure chamber. The ambient pressure inside the test chamber and the pressure chamber were reduced alternatively using the suction side of the pump, keeping the pressure difference across the diaphram very small. When the ambient pressure inside the test chamber reached the required value, air was let in inside the pressure chamber through the valve until the pressure difference across the diaphram corresponded to the required contact pressure (from equation 4.2). The end of the smaller rod was exposed to the radiant heat flux and the temperature transients were recorded as in program (i).

flexible diaphragm

test chamber

pressure chamber

P_1

P_2

a

A

cylinder

socket
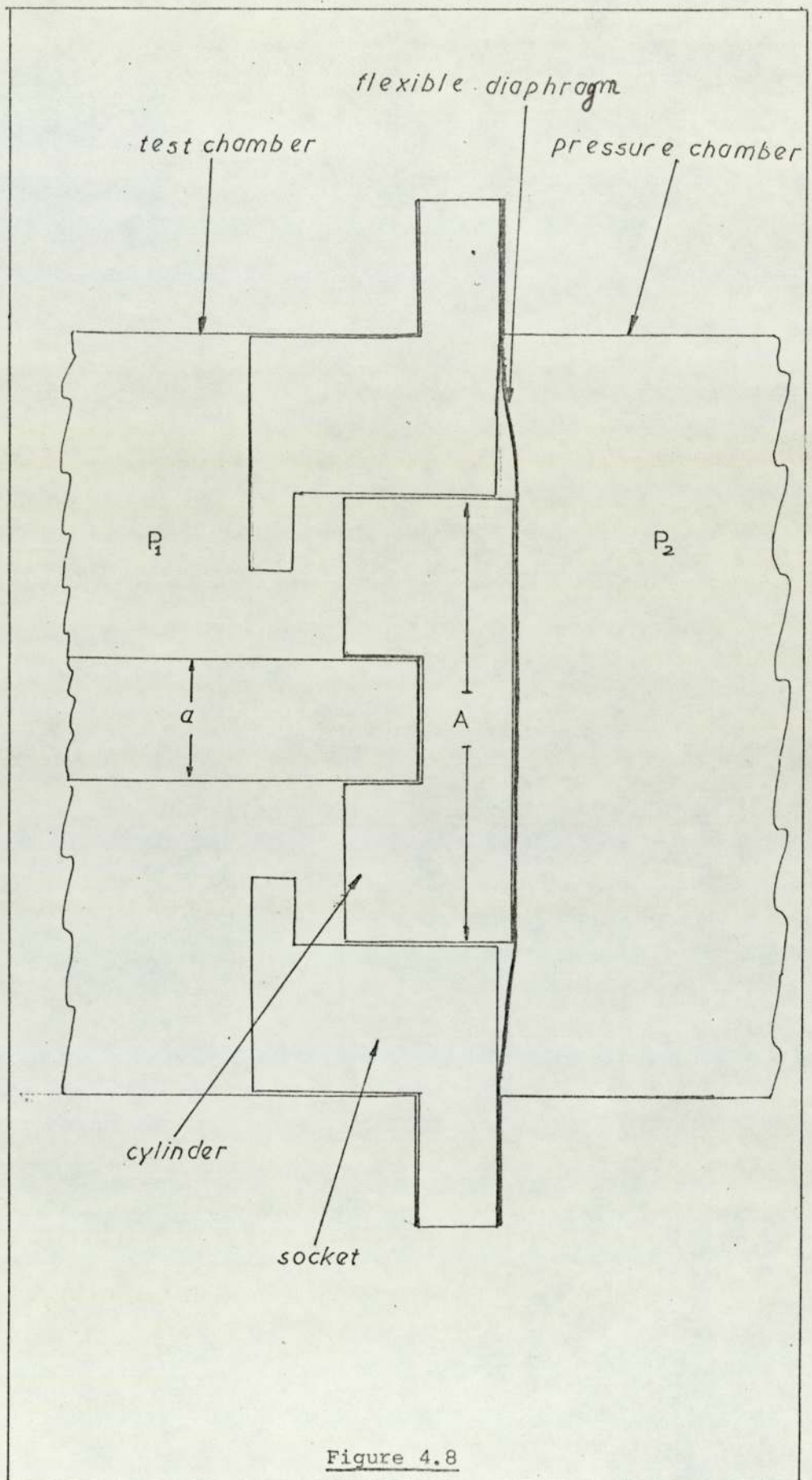
Figure 4.8

4.2.3 Analysis of Experimental Data

The temperature values were obtained from the e.m.f. values recorded using standard thermocouple data. The total time taken for each of the experiments was 30 mintes. The temperature values at three minute intervals were used for the analysis. The increase in temperature on the larger rod at the point corresponding to the nodal point 9, was found to be very small. It was therefore decided to use the temperature transients set up in the smaller rod for the analysis. The least square function was formed using these temperature values together with the coresponding theoretically predicted values evaluated by the finite difference scheme.

The information available for the thermal conductivity, K_p, of the plastic material was not adequate enough for our analysis. The aim was to evaluate the contact conductance h_c and the thermal conductivity of the plastic material, K_p, that minimises the least square function F_n, where

$$F_n = \sum_{n=1}^{10} \left[T_c (h_c, K_p) - T_{exp} \right]^2 \qquad (4.3)$$

The minimum of this function was obtained using an optimization technique based on the spiral algorithm [32]. The algorithm was devised by A. Jones, for the estimation of parameters in non-linear models. A computer program for this algorithm together with a program for the finite difference scheme to obtain the objective function was used to evaluate the parameters. All the programs were in Fortran IV and run on the University ICL 1905 computer.

The outline of the steps involved in the data reduction

1	h_c	K_p	FN = Sum of Squares
STARTING POINT	186.0	0.111	6.31
FINAL RESULT	151.97	0.10654	1.7041

2	h_c	K_p	FN
STARTING POINT	200.0	0.1065	4.027
FINAL RESULT	171.43	0.10336	1.7046

3	h_c	K_p	FN
STARTING POINT	145.0	0.1240	11.491
FINAL RESULT	116.09	0.1160	1.7031

4	h_c	K_p	FN
STARTING POINT	120.0	0.100	10.08
FINAL RESULT	147.93	0.10734	1.7041

Table 4.1

procedure is given in Appendix 4. On analysing a set of data in which

$$F_o = 1920 \text{ BTU/hr ft}^2$$

and the initial temperature of the system is 87.4^oF, the final values of contact conductance h_c and the thermal conductivity of the plastic material K_p were found to be dependent on the initial starting value in the optimization procedure. The sum of squares value obtained in each case was found to be of the same order (1.70), although the conductance h_c, and the conductivity K_p values corresponding to the apparent minimum were different (Table 4.1).

It therefore became necessary to examine the behaviour of the least squares function to see if it showed a single true minimum. The computer program written for the theoretical temperature distribution was modified by including the experimental data to calculate the value of the least square function for a range of values of conductance h_c and conductivity K_p. This enabled us to sketch the contour of the function F_n. The contour obtained by this procedure for the first set of experimental data is given in Figure 4.9. The function has no unique minimum point but has a line of minimum lying along a curved valley. This explains the results obtained from the spiral search technique.

This result required that K_p be measured independently in order to evaluate h_c. It was also observed that the line of minimum on the contour was lying almost parallel to the h_c axis at h_c values greater than about 300 BTU/hr ft^2 ^oF (1700 W/m^2 ^oK), i.e. at higher values of h_c the total resistance
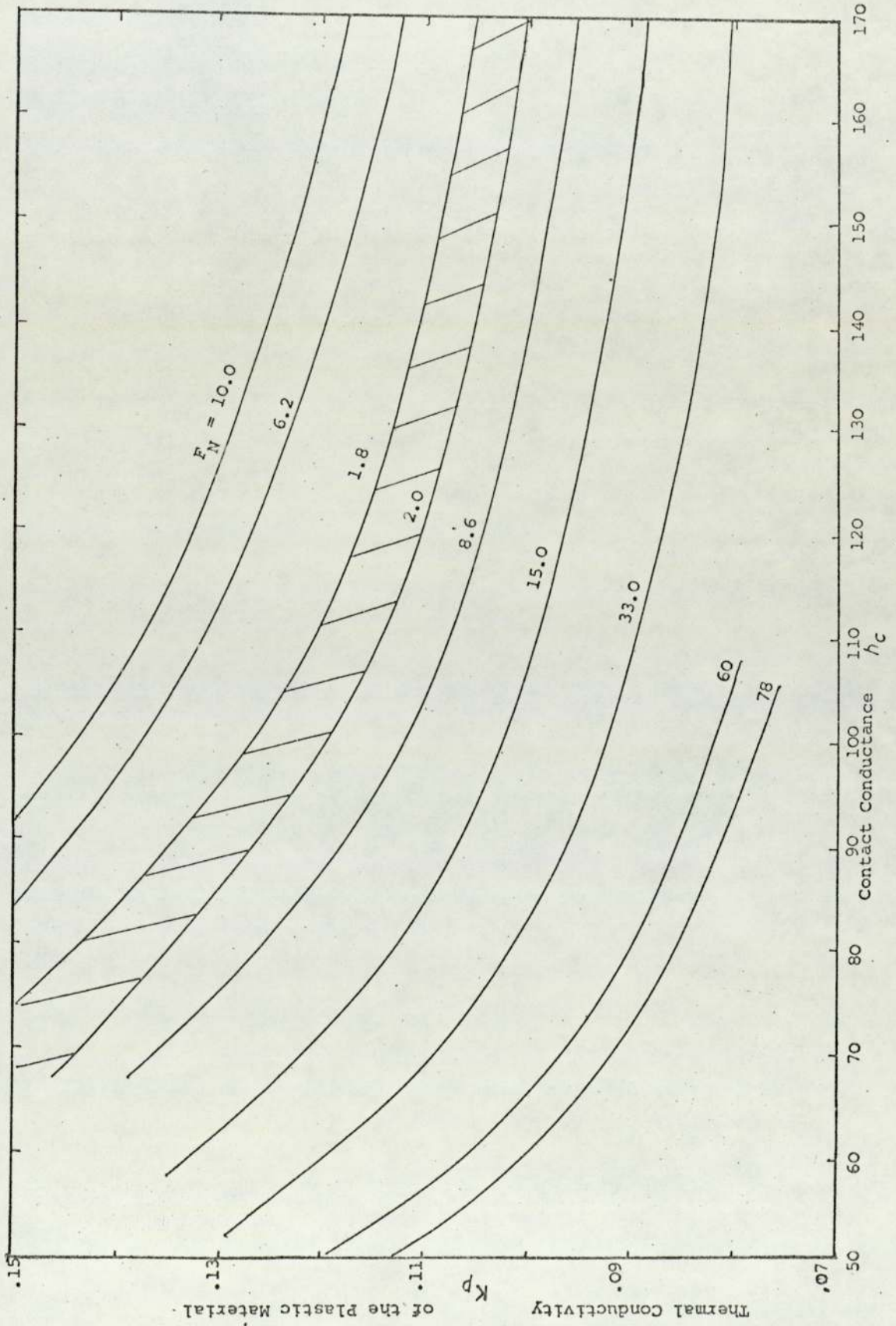
Figure 4.9   The Contour of F_N

between the metal surfaces in contact with the plastic material
can be regarded as only that due to the sandwiched plastic
material. Hence the thermal conductivity of the plastic
material K_p would be the value of K_p corresponding to large h_c
values. An alternative method was devised to obtain the K_p
value independently in order to evaluate h_c.

4.3 Alternative Method: Transient Measurements at High Contact Conductance

The aim was to achieve a high contact conductance across
the interfaces such that the total resistance across the metal
surfaces would be only that due to the plastic material sand-
wiched between them. The contact conductance should be greater
than about 300 BTU/hr ft^2 $^\circ$F. In order to achieve a conductance
value in this range, a high surface tension liquid has to be
introduced between the interfaces and high contact pressure has
to be applied. Glycerine was used for this purpose and a
contact pressure of 175 psi was applied across the contact.
The temperature transients set up in the composite system under
these conditions were obtained when the end of the smaller rod
received a previously measured radiant heat flux.

The thermal conductivity of the plastic material K_p was
evaluated by linear search technique at high values of conduc-
tance h_c (500 BTU/hr ft^2 $^\circ$F - 1,000 BTU/hr ft^2 $^\circ$F) along xy
(Figure 4.10) on the least square function formed by this
experimental data and theoretically predicted temperature
transients. Table 4.2 gives the results obtained from the
search technique.
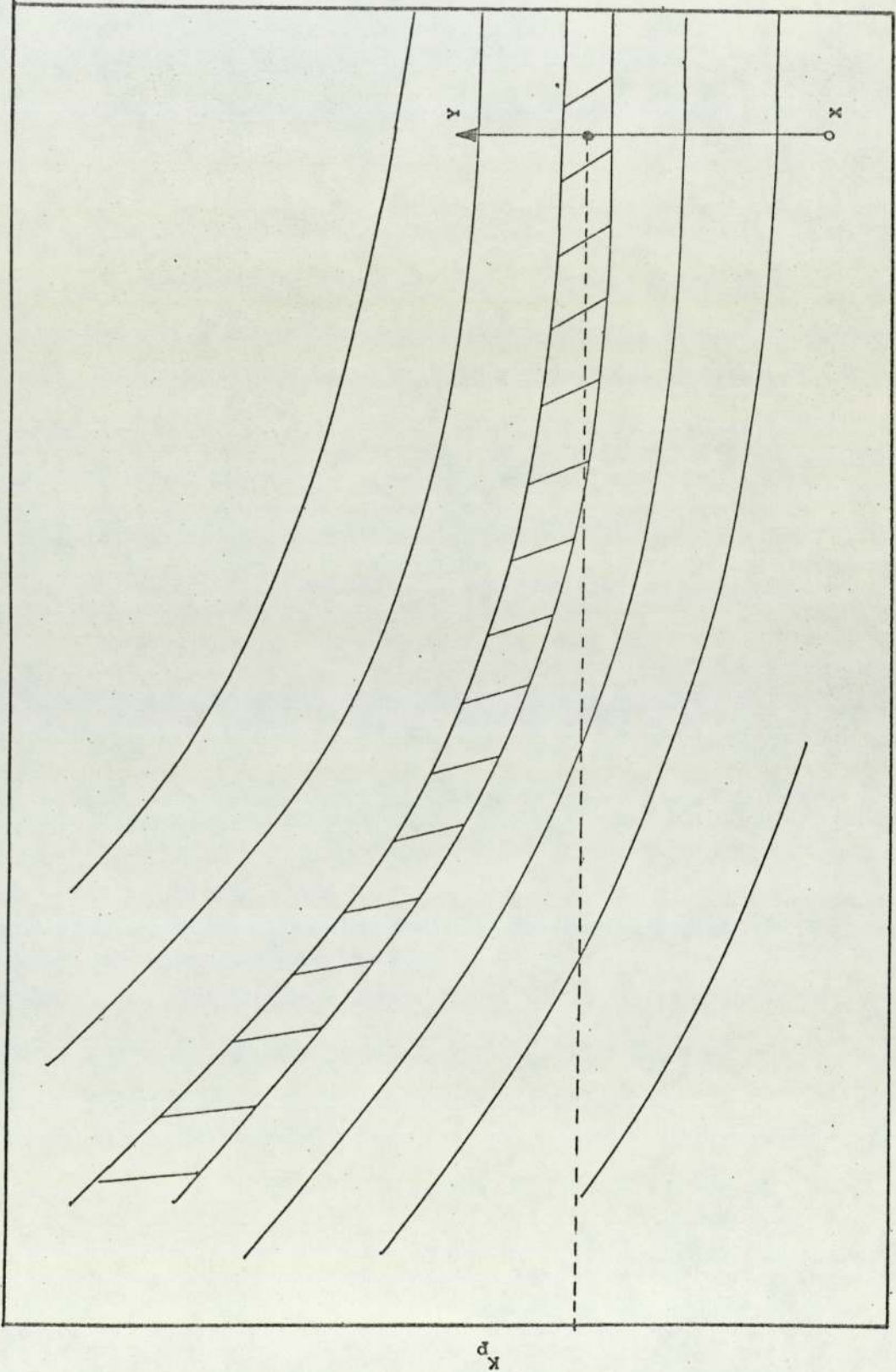
Figure 4.10   Linear Search to Evaluate K_p

h_c Value Assumed		K_p Value Obtained	
BTU/hr ft^2 ^{o}F	W/m^2 ^{o}K	BTU/hr ft ^{o}F	W/m ^{o}K
500	2839	0.1042	0.1804
1000	5678	0.1041	0.1802

Table 4.2

This suggested that K_p dominates the resistance between faces and this value of K_p can be used to evaluate h_c at lower contact pressures.

The search technique used for this evaluation was that of Davies, Swann and Campey [33]. The computer program written for this purpose based on Davies, Swann and Campey's method is given in Appendix 5. The master program consisted of the optimization technique, while the subroutine TC(F_n, X), evaluated the objective function from the theoretical and experimental temperature data.

The thermal conductivity value K_p obtained by this method was used to estimate the contact conductance h_c at lower contact pressures from curves of dimensionless temperature vs dimensionless time (Figure 3.4). The curve obtained from experimentally measured temperature values was similar in shape to those obtained from theoretically predicted values. The position where the experimental curve fits, suggested a suitable starting point for the search technique. Knowing a suitable starting point, h_c was evaluated by a linear search at constant K_p along x'y' as shown in Figure 4.11.
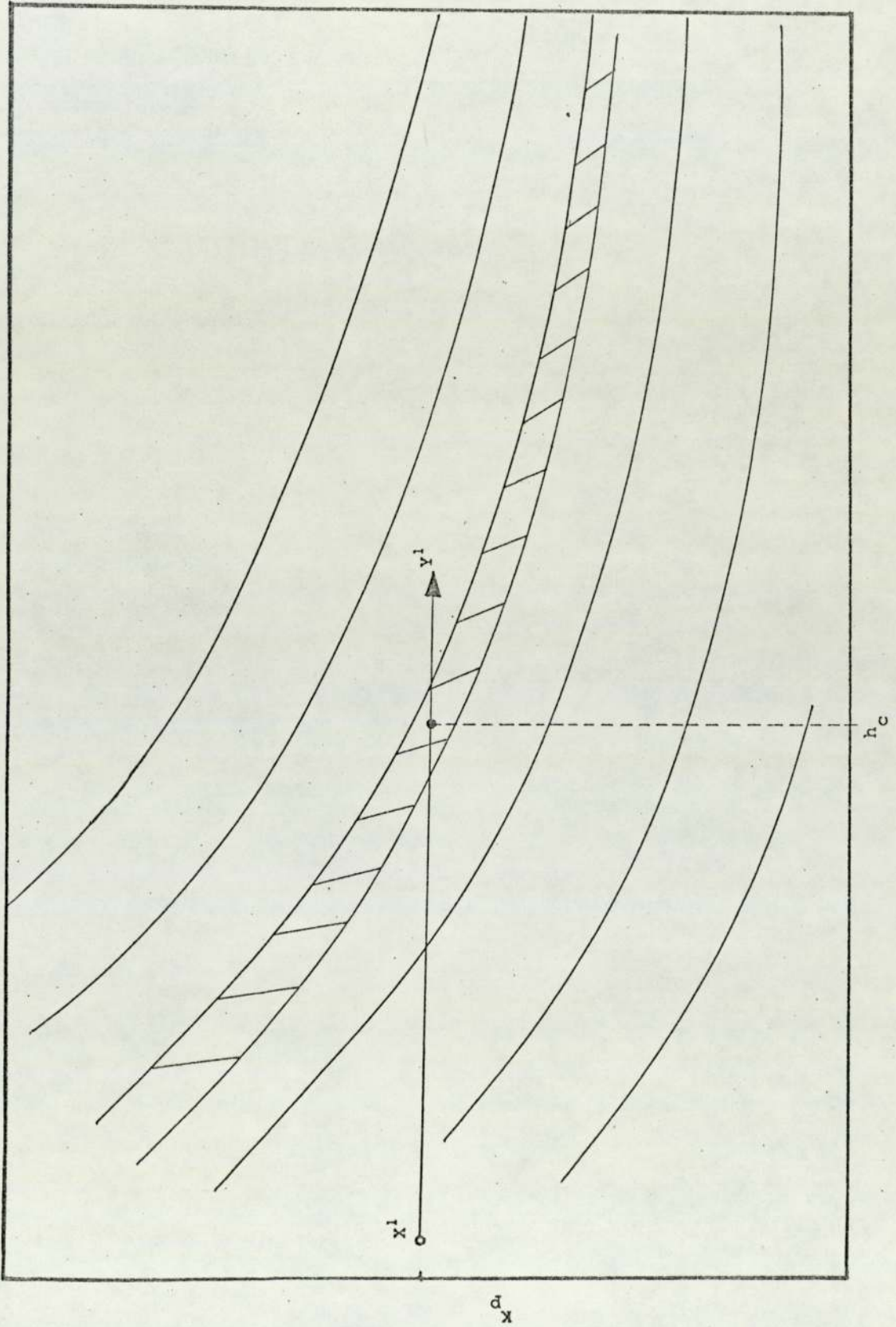
Figure 4.11 Linear Search to Evaluate h_c

S E C T I O N   5

RESULTS AND DISCUSSION

5.1 Introduction

This section presents the results obtained using the transient method developed to measure contact conductance at metal plastic interfaces and a discussion of the accuracy of measurements. The metal rods used for the measurements were HE 30 WP aluminium alloy. The plastic sheet was 'Tyril', a styrene-acrylonitrile copolymer. The physical properties of the test specimens are given in Appendix 6.

The results obtained confirm the accuracy and suitability of the method for ~~any~~ metal-plastic surfaces. However, the relationship obtained and conclusions cannot be generalised for all metal-plastic surfaces. The results obtained were based on the assumption that the physical properties of the test specimen and the contact conductance are independent of temperature. The measurements were made in the temperature range of $70^{\circ}F$ to $200^{\circ}F$.

5.2 Results

5.2.1 The Effect of Contact Pressure on Contact Conductance

The experimental results include the effect of contact pressure and ambient pressure on contact conductance. The effect of contact pressure was obtained using the experimental procedure explained in program (i), Section 4.2.2. The variation of contact conductance with the applied pressure may give information on the deformation characteristics of the plastic material. This is based on the fact that the plastic material is by far the softer of the two materials in contact and will

tend to deform into the interstitial volume. Table 5.1 gives
the variation of contact conductance h_c with contact pressure
P, when the specimens were at atmospheric pressure.

The relationship obtained between contact pressure P
and contact conductance h_c using a standard library subroutine
for curve fitting available in the University Computer Centre
was:

For p < 200 *psi*

$$h_c = 20.61 + 2.25P + 0.003 P^2 \qquad (5.1)$$

in which h_c is in BTU/hr ft^2 ^{o}F

and P is in psi.

It shows a linear relationship at contact pressures below
about 25 psi in which the term 0.003 P^2 is negligible compared
to the first two terms (equation 5.1). At higher pressures the
relationship deviates from linearity. The linear dependence of
h_c on P that our results show at lower contact pressures are
comparable to the early results of Jacob and Starr for copper
contacts (reported in [6]).

The available theories (Section 2) predict that h_c values
increase as P^n where n < 1, a response to pressure that is quite
unlike the response in our experiments. Our results suggest
that these theories are inadequate to describe contact conductance
between highly deformable surfaces.

5.2.2 The Effect of Ambient Pressure on Contact Conductance

Table 5.2 gives the results obtained by employing the
experimental procedure explained in program (ii), Section 4.2.3.

RUN NUMBER	HEAT FLUX, F_0 BTU/hr ft²	CONTACT PRESSURE psi	CONTACT CONDUCTANCE			
			DIM. ANALYSIS		OPTIMIZATION TECHNIQUE	
			BTU/hr ft² °F	W/m² °K	BTU/hr ft² °F	W/m² °K
1	1950.0	8.75	45.0	256.0	49.90	284.0
2	2190.0	25.20	60.0	341.0	57.27	326.0
3	2090.0	43.20	130.0	738.0	139.90	795.0
4	2565.0	46.00	130.0	738.0	130.00	738.0
5	2450.0	50.00	150.0	851.0	145.20	825.0
6	1920.0	64.00	175.0	994.0	166.00	943.0
7	2390.0	69.00	180.0	1020.0	193.90	1100.0

Table 5.1

RUN NUMBER	HEAT FLUX, F_o BTU/hr ft^2	AMBIENT PRESSURE psi	CONTACT CONDUCTANCE			
			DIM. ANALYSIS		OPTIMIZATION TECHNIQUE	
			BTU/hr ft^2 $^\circ$F	W/m^2 $^\circ$K	BTU/hr ft^2 $^\circ$F	W/m^2 $^\circ$K
1	1950.0	14.7	45.0	256.0	44.9	255.0
2	2510.0	10.5	50.0	284.0	58.8	334.0
3	2210.0	8.2	45.0	256.0	50.2	285.0
4	2470.0	6.2	45.0	256.0	48.0	273.0
5	2115.0	3.5	45.0	256.0	47.7	271.0

Table 5.2

Contact Pressure = 8.75 psi

It shows that ambient pressure has very little effect on contact conductance. This suggests that the solid-solid conduction mode dominates the heat transfer across the contact in the range of temperatures and pressures used in the experiments and the fluid conductance K_f/δ_f has negligible influence on contact conductance.

5.3 Experimental Accuracy

5.3.1 Introduction

The temperature measurements were made using alumel-chromel thermocouples. The e.m.f. produced by a standard alumel-chromel thermocouple at boiling point of water (100°C) was 4.10 mV, while that produced by the thermocouple used in the experiments was about 4.09 mV. Hence, the accuracy of the temperature measurements was around $\pm 0.1^\circ$C and the average error was less than 0.1%.

The contact pressure was evaluated from the mercury manometer readings to about ± 1.0 psi.

5.3.2 Accuracy of Measurement of Heat Flux

The fluctuation of furnace temperature was less than 3°C. This would produce about 0.8% error in the heat flux F_o. The effect of increase in temperature of the surface that received the radiant heat flux from the furnace on the heat flux values was estimated to be less than 0.6% (Table 3.1). Hence, the overall error in the measurement of the heat flux will be less than 1.0%. A good linear relationship was obtained between temperature T and time Θ for the heat flux measurements

(Figure 4.7). Table 5.3 gives the effect of the heat flux F_o
on two values of contact conductance h_c measured.

F_o	h_c	% change in F_o	% change in h_c
1920	166.0	1.0	~7
1950	49.9	1.0	~4

Table 5.3

The error in the heat flux measurements of about 1% is the major
source of error in the determination of contact conductance.
It produces a maximum of about 7.5% in the estimation of contact
conductance.

5.3.3 The Effect of the Accuracy of Thermal Conductivity of
       the Plastic Material K_p on Contact Conductance h_c

The thermal conductivity of the plastic material K_p was
calculated from experiments at high contact conductance (Section
4), in which the total resistance between the metal surfaces was
assumed to be only that due to the plastic material sandwiched
between them. Conductivity values of 0.1042 BTU/hr ft ^{o}F and
0.1041 BTU/hr ft ^{o}F were obtained when the contact conductance
values were assumed to be 500 BTU/hr ft^2 ^{o}F and 1000 BTU/hr ft^2 ^{o}F
respectively. The contact conductance values obtained at lower
contact pressures differ by less than 0.5% for conductivity
values of 0.1042 and 0.1041. A conductivity value of 0.1042
BTU/hr ft ^{o}F was used to evaluate contact conductance at lower
contact pressures. The error produced by assuming this value of

thermal conductivity K_p on contact conductance will be less than 1%.

The effect of the thermal conductivity value K_p on contact conductance under steady state conditions was estimated to be of the same order. The estimation was based on Figure 5.1a and 5.1b in which the contact conductance values at the two interfaces are assumed to be equal. Hence, for given heat flux Q across the interfaces, thermal conductivity K_p and contact conductance h_c, the temperature drop $(\Delta T)_1$ at the interfaces can be evaluated.

For example, if the heat flux across the interfaces is Q,

$$\text{then for } Q = 2000 \quad BTU/h\ ft^2$$
$$h_c = 100 \quad BHi/h\ ft^2\ F$$
$$\text{and } K_p = 0.1042 \quad Btu/h\ ft\ F$$

$$\text{using } Q = h(\Delta T)_1$$
$$2000 = 100 \cdot (\Delta T)_1$$
$$(\Delta T)_1 = 20 \quad F \qquad (i)$$

The temperature drop across the plastic material $(\Delta T)_2$ of thickness 0.0650 will be

$$(\Delta T)_2 = \frac{2000}{0.1042} \times .0050$$

$$(\Delta T)_2 = 95.96 \quad F$$

Hence, for $K_p = 0.1042$, the total temperature drop $(\Delta T)_t$ across the metal surfaces will be

$$(\Delta T)_t = 2(\Delta T)_1 + (\Delta T)_2$$

$$(\Delta T)_t = 135.96 \quad F$$
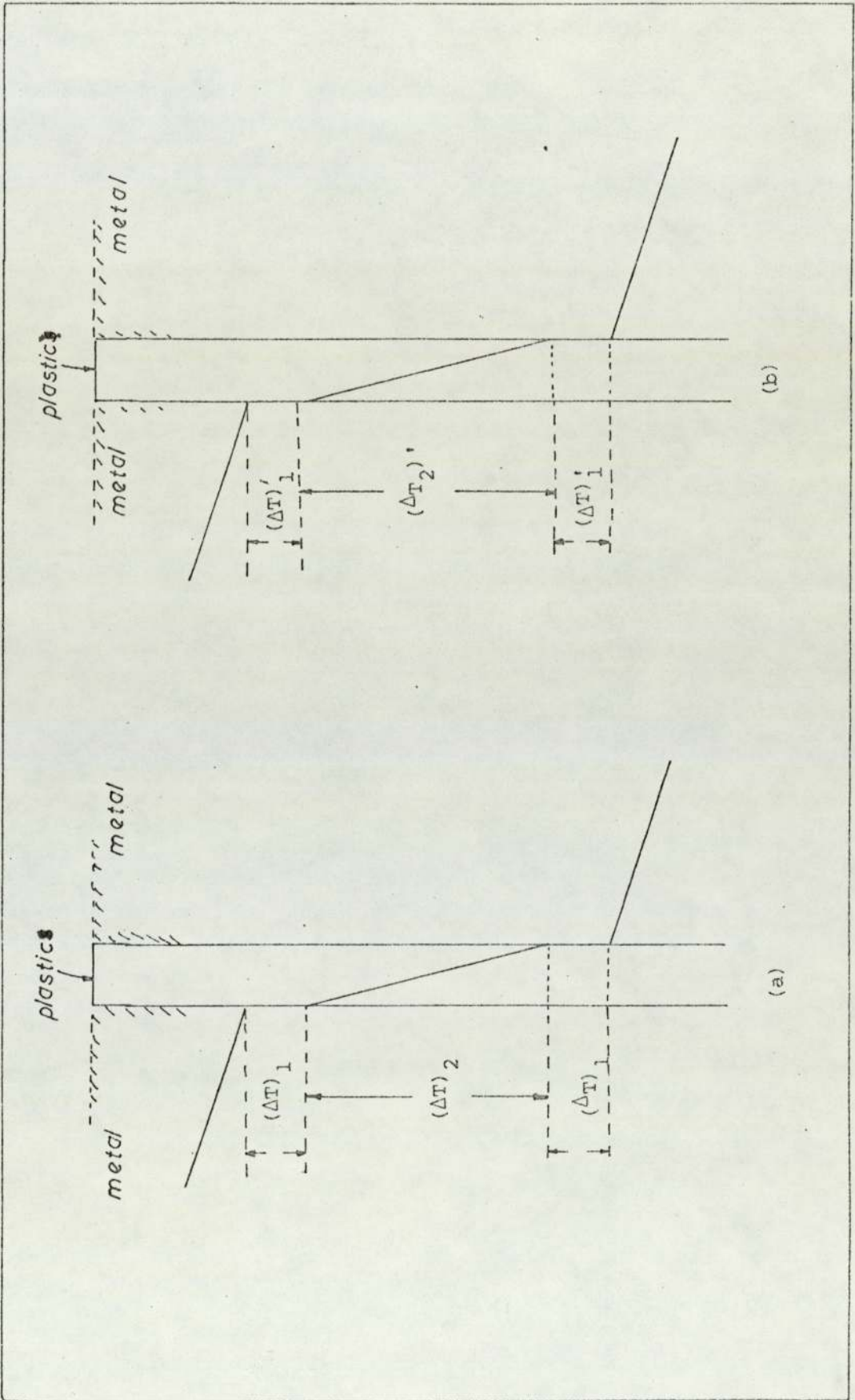
Figure 5.1 Effect of K_p under steady state conditions

If the K_p value is changed to a new value of 0.1041: $(\Delta T)'_2$

the temperature drop across the plastic material $= \dfrac{2000}{0.1041} \times .0050$

i.e. $(\Delta T)'_2 = 96.06$ F

Then the new value of $(\Delta T)_1$ becomes:

$$(\Delta T)'_1 = \frac{135.96 - 96.06}{2}$$

$$= 19.95$$

Hence, the new contact conductance value h'_c is:

$$h'_c = \frac{2000}{19.95} = 100.25 \quad Btu/h \; ft^2 \; F$$

The % change of h_c is about 0.25%.

CONCLUSIONS

Contact conductance at metal-plastic interfaces can be measured by the transient method described in the thesis to an error of not more than 10%. The major source of error in the method arose in the estimation of the radiant heat flux. The accuracy of the method can be increased with a more stable heat source.

The results obtained from our experiments for contact conductance at metal-plastic surfaces do not agree with the existing mechanisms describing contact conductance at metal-metal interfaces.

Further work should consider mechanisms to describe contact conductance between metal-plastic surfaces and measurement of temperature dependent contact conductance over a wider range of temperatures.

A P P E N D I C E S

APPENDIX 1

Evaluation of Heat Loss Correction Term by Cooling Experiments

The smaller rod 3" long, insulated with polyurethane was heated by the radiant heat flux. The radiant heat flux was suddenly removed and the rate of decrease of temperature $\partial T/\partial\Theta$ at different excess temperatures $(T - T_i)$ were observed. Theoretical studies showed that the axial flow of heat in the rod during cooling will have negligible influence on the rate of change of temperature $\partial T/\partial\Theta$ at the point in which the measurements were made. Hence, the rate of decrease of temperature $\partial T/\partial\Theta$ is assumed to be only that due to the surface loss. The range of temperature in which these experiments were carried out, covers the range in which the conductance measurements were made. The variation of the rate of decrease of temperature at various excess temperatures for the system is presented in a graphical form in Figure A.1. The relationship between $\partial T/\partial\Theta$ and $(T - T_i)$ was obtained by curve fitting. A parabola $\partial T/\partial\Theta = Q(T - T_i)^2$ fits the experimental points.

Hence, the heat conduction equation becomes:

$$\frac{\partial T}{\partial\Theta} = \alpha\frac{\partial^2 T}{\partial x^2} - Q(T - T_i)^2 \qquad (A.1)$$

$Q = 0.0342$ if T is in $^{\circ}F$ and Θ is in hours;

$Q = 1.71 \times 10^{-5}$ if T is in $^{\circ}C$ and Θ is in seconds.
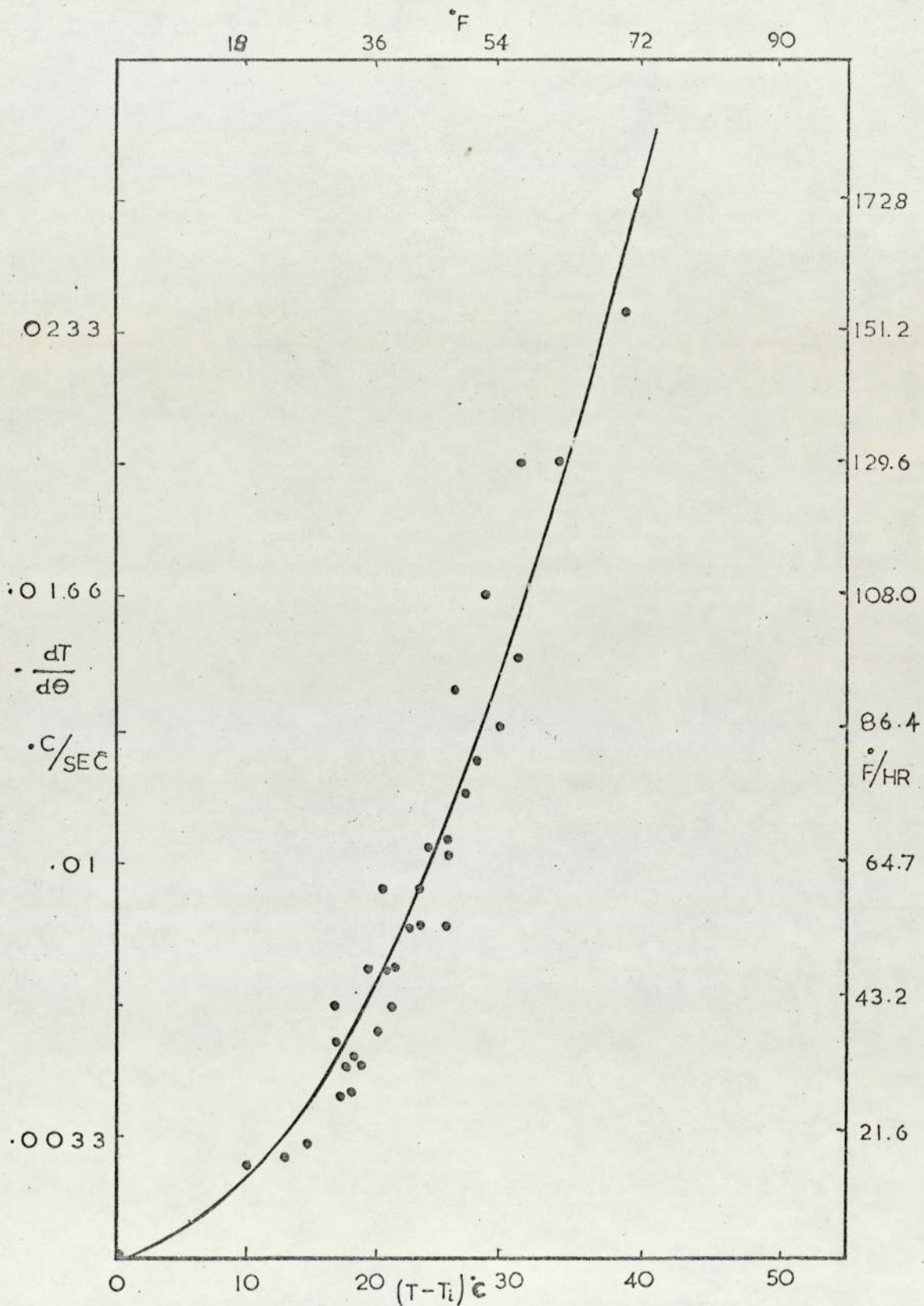
FIG A1

APPENDIX 2

A.2.1   The non-Linear Equations Obtained in Writing the Heat

Conduction Equation (A.1) in Finite Difference Form

$$Q.\Delta\theta.T^2_{1,\,\theta+\Delta\theta} + (4 \times (1) + Q.\Delta\theta(2\,T_{1,\,\theta} - 4\,T_i))T_{1,\,\theta+\Delta\theta} +$$

$$4\,Y(1).T_{2,\,\theta+\Delta\theta} = 4\,R(1) - Q.\Delta\theta(T_{1,\,\theta} - 2\,T_i)^2 \qquad (A.2)$$

For n = 2 to 10:

$$Q.\Delta\theta.T^2_{n,\,\theta+\Delta\theta} + 4\,Z(n-1).T_{n-1,\,\theta+\Delta\theta} + (4\,X(n) + Q.\Delta\theta(2\,T_{n,\,\theta} - 4\,T_i))$$

$$T_{n,\,\theta+\Delta\theta} + 4\,Y(n)\,T_{n+1,\,\theta+\Delta\theta} = 4\,R(n) - Q.\Delta\theta\,(T_{n,\theta} - 2\,T_i)^2$$

$$\qquad (A.3)$$

For n = 11:

$$Q.\Delta\theta.T^2_{11,\theta+\Delta\theta} + 4\,Z(10).T_{10,\theta+\Delta\theta} + (4\,X(11) + Q.\Delta\theta.(2\,T_{11,\theta} - 4\,T_i))$$

$$T_{11,\theta+\Delta\theta} = 4\,R(11) - Q.\Delta\theta(T_{11,\theta} - 2\,T_i)^2 \qquad (A.4)$$

in which   X(n), R(n)   n from 1 to 11

and   Y(n), Z(n)   n from 1 to 10 are defined in Section 3,

pages 30 and 31

A.2.2 <u>Newton's Iterative Method for Solving Non-Linear Simultaneous
Equations</u>

The unknown values in the set of equations A2 to A4 are
T_n, $\theta + \Delta\theta$, $n = 1$ to 11. The equations are represented by the
following:

$$f_1(T_1, T_2) = 0 \tag{A.5}$$

$$f_2(T_1, T_2, T_3) = 0 \tag{A.6}$$

For $n = 3$ to 10:

$$f_n(T_{n-1}, T_n, T_{n+1}) = 0 \tag{A.7}$$

$$f_{11}(T_{10}, T_{11}) = 0 \tag{A.8}$$

and on expanding f_n in a Taylor series in terms of an arbitrary
estimate to the desired roots $(T_n + \Delta T_n)$ for $n = 1$ to 11.

Assuming T_o and T_{12} does not exist:

$$f_n(T_{n-1} + \Delta T_{n-1})(T_n + \Delta T_n)(T_{n+1} + \Delta T_{n+1}) = 0$$

$$= f_n(T_{n-1}, T_n, T_{n+1}) + \Delta T_{n-1} \cdot \left[\frac{\partial f_n}{\partial T_{n-1}}\right] + T_n \cdot \frac{\partial f_n}{\partial T_n} +$$

$$\Delta T_{n+1} \cdot \frac{\partial f_n}{\partial T_{n+1}} + \text{higher order terms in } \Delta T \tag{A.9}$$

and assuming the higher order terms in ΔT to be small, equation A.9
becomes:

$$f_n(T_{n-1}, T_n, T_{n+1}) + \Delta T_{n-1}\frac{\partial f_n}{\partial T_{n-1}} + \Delta T_n \cdot \frac{\partial f_n}{\partial T_n} + \Delta T_{n+1} \cdot \frac{\partial f_n}{\partial T_{n+1}} = 0$$

$$\tag{A.10}$$

Hence, equation A.10 for $n = 1$ to 11, yields eleven simultaneuous

equations with respect to ΔT_n. Thus, an iteration pattern can be set up as shown in the flowchart given in Figure A.2.

Figure A.2

In the flowchart:

START

Initial guess for T_n,
$\theta + \Delta\theta$, n = 1, 11

Substitute for T_n, $\theta + \Delta\theta$
in Equation A.10
for n = 1, 11

Solve for ΔT_n, n = 1, 11
by Gauss-Jordon's method

$T_n = (T_n + \Delta T_n)$

NO

$$\sum_{n=1}^{11} (\Delta T_n)^2 < 10^{-3}$$

YES

WRITE $T_n, \theta + \Delta\theta$

A.2.3   Computer Program in Fortran IV for Solving non-Linear
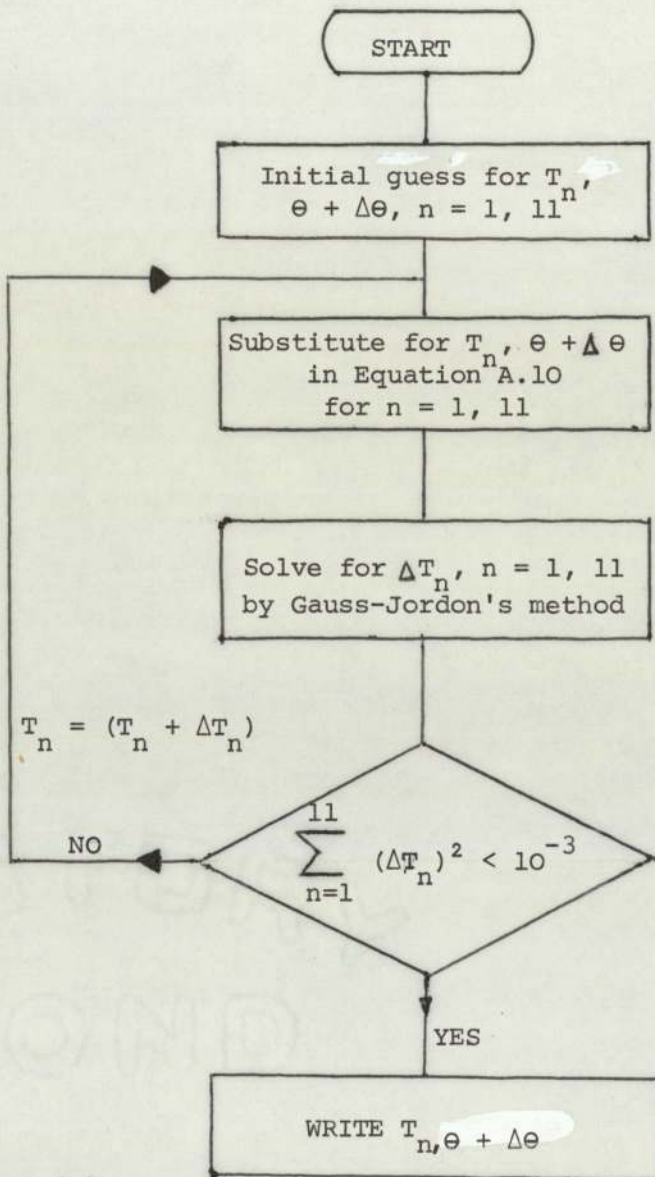
Simultaneous Equations

```
        MASTER MPCT
C       NEWTON RAPHSON ITERATION FOR NON-LINEAR SIMULTANEOUS EQNS
        DIMENSION TO(11),TN(11),X(11),Y(10),Z(10),R(11),G(11),W(11),
       1TP(11),TG(11),DI(11),S(11),DS1(11),DS2(10),DS3(10)
        REAL K1,K2,K3,M,N1,N2,N3,N4,L1,L2
        READ(1,10)(TP(I),I=1,11),FO,L1,L2,K1,K3,C1,C2,C3,
       1RHO1,RHO2,RHO3,DT,M,K2,Q,T1,H
        A1=K1/(C1*RHO1)
        A2=K2/(C2*RHO2)
        A3=K3/(C3*RHO3)
        B1=A1*DT/(L1**2.0)
        B2=A2*DT/(M**2.0)
        B3=A3*DT/(L2**2.0)
        N1=K1/(H*L1)
        N2=K2/(H*M)
        N3=N2
        N4=K3/(H*L2)
   10   FORMAT(8F10.0)
        X(1)=2.0+2.0*B1
        DO3 I=1,2
    3   X(I+1)=X(I)
        X(4)=2.0+2.0*B1+(2.0*B1/N1)
        X(5)=2.0+2.0*B2+(2.0*B2/N2)
        X(6)=2.0+2.0*B2
        X(7)=2.0+2.0*B2+(2.0*B2/N3)
        X(8)=2.0+2.0*B3+(2.0*B3/N4)
        X(9)=2.0+2.0*B3
        X(10)=2.0+2.0*B3
        X(11)=2.0+2.0*B3
        Y(1)=-2.0*B1
        Y(2)=-B1
        Y(3)=-B1
        Y(4)=-2.0*B1/N1
        Y(5)=-2.0*B2
        Y(6)=-B2
        Y(7)=-2.0*B2/N3
        Y(8)=-2.0*B3
        Y(9)=-B3
        Y(10)=-B3
        Z(1)=-B1
        Z(2)=-B1
        Z(3)=-2.0*B1
        Z(4)=-2.0*B2/N2
        Z(5)=-B2
        Z(6)=-2.0*B2
        Z(7)=-2.0*B3/N4
        Z(8)=-B3
        Z(9)=-B3
        Z(10)=-2.0*B3
        SUM=0.0
        IC=0
        DO21 I=1,11
        TO(I)=TP(I)
        TG(I)=TP(I)
   21   CONTINUE
        DO8 II=1,80
```

```
      R(1)=(2.0-2.0*B1)*TO(1)+2.0*B1*(TO(2)+(2.0*FO*L1/K1))
      R(2)=B1*TO(1)+(2.0-2.0*B1)*TO(2)+B1*TO(3)
      R(3)=B1*TO(2)+(2.0-2.0*B1)*TO(3)+B1*TO(4)
      R(4)=2.0*B1*TO(3)+(2.0-2.0*B1-(2.0*B1/N1))*TO(4)+((2.0*B1
     1/N1)*TO(5))
      R(5)=(2.0*B2/N2)*TO(4)+(2.0-2.0*B2-(2.0*B2/N2))*TO(5)+2.0*
     1B2*TO(6)
      R(6)=B2*TO(5)+(2.0-2.0*B2)*TO(6)+B2*TO(7)
      R(7)=2.0*B2*TO(6)+(2.0-2.0*B2-(2.0*B2/N3))*TO(7)+(2.0*B2/N3
     1)*TO(8)
      R(8)=(2.0*B3/N4)*TO(7)+(2.0-2.0*B3-(2.0*B3/N4))*TO(8)+2.0*B3
     1*TO(9)
      R(9)=B3*TO(8)+(2.0-2.0*B3)*TO(9)+B3*TO(10)
      R(10)=B3*TO(9)+(2.0-2.0*B3)*TO(10)+B3*TO(11)
      R(11)=2.0*B3*TO(10)+(2.0-2.0*B3)*TO(11)
   29 S(1)=Q*DT*TG(1)**2+(4.*X(1)+Q*DT*(2.*TO(1)-4.*T1))*TG(1)
     1+4.*Y(1)*TG(2)-4.*R(1)+Q*DT*(TO(1)-2.*T1)**2
      DO12 I=2,10
   12 S(I)=Q*DT*TG(I)**2.+(4.*Z(I-1))*TG(I-1)+(4.*X(I)+Q*DT*
     1(2.*TO(I)-4.*T1))*TG(I)+4.*Y(I)*TG(I+1)-4.*R(I)+Q*DT*
     2(TO(I)-2.*T1)**2
      S(11)=Q*DT*TG(11)**2+4.*Z(10)*TG(10)+(4.*X(11)+Q*DT*(2.*TO(11)
     1-4.*T1))*TG(11)-4.*R(11)+Q*DT*(TO(11)-2.*T1)**2
      DS1(1)=2.*Q*DT*TG(1)+4.*X(1)+Q*DT*(2.*TO(1)-4.*T1)
      DS2(1)=4.*Y(1)
      DS3(1)=4.*Z(1)
      DO9 I=2,10
      DS3(I)=4.*Z(I)
      DS1(I)=2.*Q*DT*TG(I)+4.*X(I)+Q*DT*(2.*TO(I)-4.*T1)
      DS2(I)=4.*Y(I)
    9 CONTINUE
      DS1(11)=2.*Q*DT*TG(11)+4.*X(11)+Q*DT*(2.*TO(11)-4.*T1)
      W(1)=DS1(1)
      G(1)=-S(1)/W(1)
      DO16 I=2,11
      W(I)=DS1(I)-(DS3(I-1)*(DS2(I-1)/W(I-1)))
      G(I)=(-S(I)-DS3(I-1)*G(I-1))/W(I)
   16 CONTINUE
      DI(11)=G(11)
      DO17 J=1,10
      I=11-J
      DI(I)=G(I)-((DS2(I)/W(I))*DI(I+1))
   17 CONTINUE
      WRITE(2,22)(DI(I),I=1,11)
   22 FORMAT(4X,6F10.5,/,4X,5F10.5//)
      DO18 I=1,11
      SUM=SUM+DI(I)**2
   18 CONTINUE
      IF(SUM-0.0001)26,27,27
   27 DO30 I=1,11
   30 TG(I)=TG(I)+DI(I)
      SUM=0.0
      GOTO 29
   26 DO31 I=1,11
   31 TN(I)=TG(I)
      DO39 I=1,11
      TO(I)=TN(I)
      TG(I)=TN(I)
```

```
   39   CONTINUE
        IC=IC+1
        IF(IC-5)8,97,97
   97   IC=0
        SUM=0.0
        WRITE(2,20)(TN(I),I=1,11)
   20   FORMAT(4X,6F10.3,/,4X,5F10.3)
    8   CONTINUE
        STOP
        END
        FINISH
```

APPENDIX 3

A.3.1 Computer Program in Fortran IV to Evaluate Temperature

Profiles using Gauss Jordon's Technique

```
      MASTER MPCT
C     IMPLICIT METHOD
      DIMENSION TO(11),TN(11),X(11),Y(10),Z(10),R(11),G(11),W(11)
     1,TP(11)
      REAL K1,K2,K3,M,N1,N2,N3,N4,L1,L2
      READ(1,10)(TP(I),I=1,11),FO,L1,L2,K1,K3,C1,C2,C3,
     1RHO1,RHO2,RHO3,DT,M,K2,Q,T1
      H=30.0
      DO18 ID=1,10
      N=1
      A1=K1/(C1*RHO1)
      A2=K2/(C2*RHO2)
      A3=K3/(C3*RHO3)
      B1=A1*DT/(L1**2.0)
      B2=A2*DT/(M**2.0)
      B3=A3*DT/(L2**2.0)
      N1=K1/(H*L1)
      N2=K2/(H*M)
      N3=N2
      N4=K3/(H*L2)
   10 FORMAT(8F10.0)
      DIMH=2.0*H*M/K2
      WRITE(2,71)DIMH
   71 FORMAT(//4X,5HDIMH=,F10.4,/,4X,15H***************)
      WRITE(2,70)
   70 FORMAT(///4X,24HTEMPERATURE DISTRIBUTION,53X,8HDIM.TEMP,6X,
     18HDIM.TIME,/4X,24H**********  **********,53X,8H********,6X,
     28H********)
      X(1)=2.0+2.0*B1
      DO3 I=1,2
    3 X(I+1)=X(I)
      X(4)=2.0+2.0*B1+(2.0*B1/N1)
      X(5)=2.0+2.0*B2+(2.0*B2/N2)
      X(6)=2.0+2.0*B2
      X(7)=2.0+2.0*B2+(2.0*B2/N3)
      X(8)=2.0+2.0*B3+(2.0*B3/N4)
      X(9)=2.0+2.0*B3
      X(10)=2.0+2.0*B3
      X(11)=2.0+2.0*B3
      Y(1)=-2.0*B1
      Y(2)=-B1
      Y(3)=-B1
      Y(4)=-2.0*B1/N1
      Y(5)=-2.0*B2
      Y(6)=-B2
      Y(7)=-2.0*B2/N3
      Y(8)=-2.0*B3
      Y(9)=-B3
      Y(10)=-B3
      Z(1)=-B1
      Z(2)=-B1
      Z(3)=-2.0*B1
      Z(4)=-2.0*B2/N2
      Z(5)=-B2
      Z(6)=-2.0*B2
```

```
      Z(7)=-2.0*B3/N4
      Z(8)=-B3
      Z(9)=-B3
      Z(10)=-2.0*B3
      IC=0
      DO21 I=1,11
   21 TO(I)=TP(I)
      DO8 II=1,80
      R(1)=(2.0-2.0*B1)*TO(1)+2.0*B1*(TO(2)+(2.0*FO*L1/K1))
     1-Q*DT*(TO(1)-T1)**2
      R(2)=B1*TO(1)+(2.0-2.0*B1)*TO(2)+B1*TO(3)
     1-Q*DT*(TO(2)-T1)**2
      R(3)=B1*TO(2)+(2.0-2.0*B1)*TO(3)+B1*TO(4)
     1-Q*DT*(TO(3)-T1)**2
      R(4)=2.0*B1*TO(3)+(2.0-2.0*B1-(2.0*B1/N1))*TO(4)+((2.0*B1
     1/N1)*TO(5))
     2-Q*DT*(TO(4)-T1)**2
      R(5)=(2.0*B2/N2)*TO(4)+(2.0-2.0*B2-(2.0*B2/N2))*TO(5)+2.0*
     1B2*TO(6)
      R(6)=B2*TO(5)+(2.0-2.0*B2)*TO(6)+B2*TO(7)
      R(7)=2.0*B2*TO(6)+(2.0-2.0*B2-(2.0*B2/N3))*TO(7)+(2.0*B2/N3
     1)*TO(8)
      R(8)=(2.0*B3/N4)*TO(7)+(2.0-2.0*B3-(2.0*B3/N4))*TO(8)+2.0*B3
     1*TO(9)
     2-Q*DT*(TO(8)-T1)**2
      R(9)=B3*TO(8)+(2.0-2.0*B3)*TO(9)+B3*TO(10)
     1-Q*DT*(TO(9)-T1)**2
      R(10)=B3*TO(9)+(2.0-2.0*B3)*TO(10)+B3*TO(11)
     1-Q*DT*(TO(10)-T1)**2
      R(11)=2.0*B3*TO(10)+(2.0-2.0*B3)*TO(11)
     1-Q*DT*(TO(11)-T1)**2
      W(1)=X(1)
      G(1)=R(1)/W(1)
      DO12 I=2,11
      W(I)=X(I)-(Z(I-1)*(Y(I-1)/W(I-1)))
      G(I)=(R(I)-Z(I-1)*G(I-1))/W(I)
   12 CONTINUE
      TN(11)=G(11)
      DO13 J=1,10
      I=11-J
      TN(I)=G(I)-((Y(I)/W(I))*TN(I+1))
   13 CONTINUE
      DO14 I=1,11
   14 TO(I)=TN(I)
      IC=IC+1
      DMTP=K1*(TN(2))/(FO*2.0*M)
      DMTE=.03125*N*A1/(4.0*M**2.0)
      IF(IC-5)8,16,16
   16 IC=0
      WRITE(2,20)(TN(I),I=1,11),DMTP,DMTE
      N=N+1
    8 CONTINUE
      H=H+15.0
   18 CONTINUE
   20 FORMAT(1H0,4X,6F10.3,/,4X,5F10.3,22X,F9.3,6X,F9.3///)
      STOP
      END
      FINISH
```

A.3.2 Comparison of the Temperature Profiles Obtained by Newton-Raphson's Method and the Alternative Method

Number of Time Increments	Temperature Values Predicted, $(T_{2,\theta})$	
	Newton Raphson's Method	Alternative Method
5	94.295	94.296
10	100.733	100.747
15	106.792	106.810
20	112.504	112.532
25	117.852	117.894
30	122.836	122.891
35	127.457	127.526
40	131.724	131.806
45	135.648	135.741
50	139.244	139.347
55	142.529	142.640
60	145.521	145.639
65	148.241	148.364
70	150.708	150.834
75	152.942	153.069
80	154.962	155.090

The 80 time increments correspond to one-half hour.

Data F_0 = 1920   BTU / h ft²

T_i = 87.4   F

Physical properties: see p 91

Dimensions see pp 27 and 48

APPENDIX 4

Outline of the Steps Involved in the Data Reduction Procedure:

    (i) Read in the initial temperature distribution of the system the heat flux at $x = o$, thermophysical and physical properties of the test specimens and the time step $\Delta\theta$.

   (ii) Read in the measured temperature values at the end of every three minutes.

 (iii) Read in initial starting point for the optimization procedure.

  (iv) Calculation of the theoretical temperature transients by the program.

   (v) Calculation of the least squares function - the objective function.

  (vi) Search for the minimum point.

 (vii) If minimum point is reached, print out the values h_c and K_p.

APPENDIX 5

Computer Program for Davies, Swann and Campey's Search Technique

```
        MASTER DSMD
C       DIRECTSEARCH
C       CONTACT RESISTANCE
        DIMENSION TO(11),TN(11),X(11),Y(10),Z(10),R(11),G(11),W(11)
       1,TP(11),EXP1(10)
        REAL K1,K2,K3,M,N1,N2,N3,N4,L1,L2
        COMMON TP,FO,L1,L2,M,C1,C2,C3,RHO1,RHO2,RHO3,DT,EXP1,
       1K1,K2,K3,TN,Q,H,T1
        READ(1,90)(TP(I),I=1,11),FO,L1,L2,K1,K3,C1,C2,C3,
       1RHO1,RHO2,RHO3,DT,M,K2,Q,T1
   90   FORMAT(8F10.0)
        READ(1,91)(EXP1(I),I=1,10)
   91   FORMAT(8F10.0)
        H=30.0
        P=H
        DP=5.0
        CALL TC(FN,P)
        U1=FN
        P1=P
        DP=2.0*DP
        P=P+DP
        H=P
        CALL TC(FN,P)
        U2=FN
        P2=P
    3   DP=2.0*DP
        P=P+DP
        H=P
        CALL TC(FN,P)
        U3=FN
        P3=P
        IF(U3-U2)4,4,5
    4   U1=U2
        P1=P2
        U2=U3
        P2=P3
        GOTO3
    5   P=P-(DP/2.0)
        H=P
        CALL TC(FN,P)
        P4=P
        U4=FN
        IF(U4-U2)6,6,7
    6   U1=U2
        P1=P2
        U2=U4
        P2=P4
        GOTO8
    7   U3=U4
        P3=P4
    8   PQ=P2+((P2-P1)*(U1-U3)/(U1-2.0*U2+U3))*2.0
   12   IF(ABS(PQ-P1).LE.3.000)GOTO21
        IF(ABS(PQ-P2).LE.3.000)GOTO22
        IF(ABS(PQ-P3).LE.3.000)GOTO23
        P=PQ
        H=P
```

```
      CALL TC(FN,P)
      UQ=FN
      IF(PQ.LT.P2.AND.UQ.LT.U2)GOTO9
      IF(PQ.LT.P2.AND.UQ.GT.U2)GOTO13
      IF(PQ.GT.P2.AND.UQ.GT.U2)GOTO14
      PA=P2
      UA=U2
      PB=P3
      UB=U3
      GOTO11
   9  PA=P1
      UA=U1
      PB=P2
      UB=U2
      GOTO11
  13  PA=PQ
      UA=UQ
      PQ=P2
      UQ=U2
      PB=P3
      UB=U3
      GOTO11
  14  PA=P1
      UA=U1
      PB=PQ
      UB=UQ
      PQ=P2
      UQ=U2
  11  PR=((PA**2.0-PB**2.0)*UQ+(PB**2.0-PQ**2.0)*UA+(PQ**2.0-PA**2.0)
     1*UB)/(2.0*((PA-PB)*UQ+(PB-PQ)*UA+(PQ-PA)*UB))
      P=PR
      H=P
      CALL TC(FN,P)
      UR=FN
      P2=PQ
      U2=UQ
      P3=PB
      U3=UB
      PQ=PR
      UQ=UR
      P1=PA
      U1=UA
      GOTO12
  21  ZF=P1
      GOTO24
  22  ZF=P2
      GOTO24
  23  ZF=P3
  24  WRITE(2,20)ZF
  20  FORMAT(2X,F10.4)
      STOP
      END
      FINISH
```

APPENDIX 6

The Properties of the Test Specimens

Manufacturers: Deutsch & Brenner Ltd, Birmingham

(i) The Metal Rods (HE 30 WP Aluminium Alloy)

Composition of the alloy:

Constituents	Percentage Nominal Composition
Aluminium	97.3
Magnesium	1.0
Silicon	1.0
Manganese	0.7

Thermophysical properties:

Density: 169.0 lb/ft^3

Specific heat: 0.213 BTU/lb $^\circ$F

Thermal conductivity: 103.0 BTU/hr ft $^\circ$F

(ii) The Plastic Material

Tyril 767, Styrene acrylonitrile copolymer

Manufacturers: Distrene Ltd, London

Density: 67.5 lb/ft^3

Specific heat: 0.330 BTU/lb $^\circ$F

Thermal conductivity: 0.1042* BTU/ h ft F

*Estimated from our experimental data.

BIBLIOGRAPHY

1. BECK, J.V. "Transient Determination of Thermal Properties"
    Nuclear Engineering and Design, 3, 373-381, 1966.

2. CARSLAW, H.S. and JAEGAR, I.C., Conduction of Heat in Solids
    p.112, Oxford, 1959.

3. CETINKLE, T.N. and FISHENDEN, M. "Thermal Conductance of Metal
    Surfaces in Contact", General Discussion on Heat Transfer,
    Proc.I.Mech.E. and ASME, London, England, 271-275, 1951.

4. CHAPMAN, A.J. "Heat Transfer", The Macmillan Co., New York,
    1960.

5. CLAUSING, A.M. and CHAO, B.T. "Thermal Contact Resistance in
    a Vacuum Environment", J.Heat Transfer, 87, No.2, p.243,
    May 1965.

6. CLIFFORD, J. Moore Jr., "Heat Transfer Across Surfaces in
    Contact: Studies of Transients in One-dimensional
    Composite Systems", Southern Methodist University,
    PhD Thesis, March 1967.

7. COOPER, M.G., MIKIE, B.B. and YOVANOVICH, M.M. "Thermal
    Contact Conductance", Int.J.Heat & Mass Transfer, 12,
    279-300, 1969.

8. DAVIES, W. "Thermal Transients in Graphite-Copper Contacts"
    Brit.J.Applied Physics, 10, 516-522, December 1959.

9. DUSINBERRE, "Heat Transfer Calculations by Finite Differences"
    Int.Text Book Co.

10. FENECH, H. and ROHSENOW, W.M. "Prediction of Thermal Conduc-
    tance of Metallic Surfaces in Contact", J.Heat Transfer,
    85, No.1, 25-24, February 1963.

11. FRIED, E. "Thermal Conduction Contribution of Heat Transfer
    at Contacts", Thermal Conductivity, 2, Edited by
    R.P. Tye, Academic Press, London & New York, 1969.

12. HEASLEY, J.H. "Transient Heat Flow Between Contacting
    Solids", Int.J.Heat & Mass Transfer, 8, No.1, 147-154,
    Pergamon Press, 1965.

13. Ho and TAYLOR, "The Effect of Physically Absorbed Gases on
    Thermal Contact Resistance", Proc.8th Conf.Thermal
    Conductivity, Indiana 1968, Plenum Press 1969.

14. HO and TAYLOR, "Temperature Dependence of Thermal Contact
    Resistance Across non-Metallic Interfaces" Proc.8th
    Conf.Thermal Conductivity, NBS Spec.Publ. 1969.

15. HORVAY, G. and EDSALL, R.H. "The Interface Temperature of
    Two Media in Poor Thermal Contact", Trans.Metallurgical
    Society of AIME, 218, No.5, 927-933, October 1960.

16. HSIEH, C.K. and YOULONKIAN, Y.S. "Correlation and Prediction
    of Thermal Contact Conductance for Normally Flat Surfaces"
    Proc.8th Conf.Thermal Conductivity.

17. JAMES V. BECK "Determination of Optimum, Transient Experiments
    for Thermal Contact Conductance" Int.J.Heat & Mass
    Transfer, 12, 621-633, 1969.

18. LAMING, L.C. "Thermal Conductance of Machined Metal Contacts"
    Proc.Int.Heat Transfer Conf., Part 1, No.8, 65-76,
    Boulder, Colorado, September 1961.

19. LAPIDUS, L. "Digital Computation for Chemical Engineers"
    McGraw-Hill.

20. CAMERON, P.T. "Computer Methods for the Heat Conduction
    Equation", PhD Thesis, University of Aston in Birmingham
    Nov.1967.

21. PNUELI, D. "An Experimental Procedure to Measure Heat
         Transfer Coefficients between non-Identical Metal
         Surfaces in Contact", Israel Journal of Technology $\underline{9}$,
         No.4, 345-348, 1971.

22. RICHARD C. BAILIE and LIANG-TSENGFAN, "Temperature Transient
         After Contact Heating", Int.J.Heat & Mass Transfer, $\underline{6}$,
         No.10, 926-927, October 1963.

23. SANOKAWA, K. "Heat Transfer Between Metallic Surfaces in
         Contact", Bulletin Japanese Soc.Mech.Engrs. $\underline{II}$, No.44,
         April 1968, 253-293.

24. SHRETS, I.T. and DYBAN, E.P. "Contact Heat Transfer Between
         Plane Metal Surfaces" Int.Chemical Engineering, $\underline{4}$,
         No.4, 621-624, October 1964.

25. TIENL, C.L. "A Correlation for Thermal Contact Conductance
         of Normally Flat Surfaces in a Vacuum" Proc.7th Conf.
         Thermal Conductivity, NBS Spec.Publ.302, 1968.

26. WILLIAMS, S. "Heat Transfer Across Metallic Joints"
         Mech.Eng. & Chem.Eng.Transactions, November 1968.

27. AEROSPACE STRUCTURAL METAL HANDBOOK, $\underline{11}$, Syracuse University
         Press, New York 1966.

28. METALS REFERENCE BOOK, Smithells, $\underline{3}$, Butterworths London 1967.

29. POPOV, V.M. and YANIN, L.F. "Heat Transfer During Contact of
         Machined Metal Surfaces with Waviness and Microroughness"
         Heat Transfer, Soviet Research, $\underline{4}$, No.2, 162-167,
         March-April 1972.

30. BOESCHOTEN, F. and van der HELD, E. "The Thermal Conductance
         of Contacts Between Aluminium and Metals", Physica, $\underline{23}$,
         34-44, 1957.

31.   WATSON, T.W. and ROBINSON, H.E.   "Thermal Conductivity of
         Some Commercial Iron-Nickel Alloys", J.Heat Transfer,
         83, No.4, 403-408, November 1961.

32.   JONES, A.   "Spiral - A New Algorithm for non-Linear Parameter
         Estimation Using Least Squares", The Computer Journal,
         13, No.3, 301-308, August 1970.

33.   BOX, M.I., DAVIES, D. and SWANN, W.H.   "Non-Linear Optimiza-
         tion Techniques" Monograph No.5, 14-15, ICI Publ.1969.

34.   HOLM, R. Electrical Contacts, Handbook, Springer Verlag,
         Berlin, Third Ed., 1958.